Efficiency Optimal Control of Interior permanent Magnet Synchronous Motor

By

Fasil Abera

SUBMITTED IN PARTIAL FULFILLMENT OF THE

REQUIREMENTS FOR THE DEGREE OF

MASTER OF SCIENCE

AT

LAKEHEAD UNIVERSITY

THUNDER BAY, ONTARIO

January 2009

Library and
Archives Canada

Published Heritage
Branch

395 Wellington Street
Ottawa ON K1A 0N4
Canada

Bibliothèque et
Archives Canada

Direction du
Patrimoine de l'édition

395, rue Wellington
Ottawa ON K1A 0N4
Canada

Your file Votre référence
ISBN: 978-0-494-49952-8
Our file Notre référence
ISBN: 978-0-494-49952-8

Table of Contents

Acknowledgment

I would like to sincerely thank my supervisor Dr. M. Nasir Uddin and co- supervisor Dr. Kristnamurty Natrajan for their guidance and encouragement throughout the program. This work would not have been possible without their support. I would also like to thank the Faculty of graduate studies and the faculty of Engineering at Lakehead University, faculty members, staff members, and my fellow graduate students for their support throughout the program. Finally, I would like to thank my families, especially Dina Mesfin, Lwei Fasil and Ruth Fasil for their patience and support.

Abstract

There has been a growing concern over energy consumption since the past decade mainly because of the soaring cost of energy and tight environmental laws and regulations. In this thesis a model based efficiency optimization for speed control of interior permanent magnet synchronous motor (IPMSM) is proposed to improve the efficiency of the motor drive which usually operates at different load and speed conditions. Recently, the IPMSM has been becoming popular due to some of its advantages such as high efficiency, high power density, low noise and robustness as compared to the conventional induction and other ac motors. Thus, the IPMSM is considered in this work. The proposed energy optimization algorithm is developed based on motor model. In order to minimize the controllable losses, the air gap flux level should be optimized. In an IPMSM the flux level can only be optimized by controlling the d-axis armature current as the field flux is supplied by the rotor permanent magnet. For the proposed work the vector control technique is used in order to achieve fast and accurate speed response, quick recovery of speed from any disturbance and insensitivity to parameter variations etc. A simulation model for the complete closed loop vector control of IPMSM incorporating the proposed energy optimization algorithm has been developed using Matlab/Simulink software. The performance of the drive has been tested extensively for different dynamic operating conditions such as sudden load, command speed and parameter changes. An efficiency gain of about 4% is obtained from the proposed optimization algorithm from simulation. After the satisfactory simulation results are found a real time implementation of the complete drive system using DSP board (DS1104) for a laboratory 5 hp motor performed and the real time responses confirms with the simulation results as expected.

List of Acronyms

AC	Alternating current
DSP	Digital signal processor
IPMSM	Interior Permanent Magnet Synchronous Motor
MMF	Magneto motive force
PI	Proportional Integral
PID	Proportional Integral Derivative
PM	Permanent Magnet
PMSM	Permanent Magnet Synchronous Motor
PWM	Pulse Width Modulation
RTI	Real Time Interface
SynRM	Synchronous reluctance motor
VSI	Voltage Source Inverter

List of Symbols

v_a, v_b, v_c	a, b and c phase voltages
v_a^*, v_b^*, v_c^*	command a, b and c phase voltages
i_a, i_b, i_c	a, b and c phase currents
i_a^*, i_b^*, i_c^*	command a, b and c phase currents
v_d	d-axis voltage
v_q	q-axis voltage
i_d	d-axis current
i_q	q-axis current
i_q^*	q-axis command current
i_d^*	d-axis command current
R_a	stator resistance per phase
L_d	d-axis inductance
L_q	q-axis inductance
L_{md}	d-axis magnetizing inductance
L_{mq}	q-axis magnetizing inductance
ω_r	rotor speed
ω_e^*	electrical speed

θ_r	rotor position
P	number of pole pairs
T_e	developed electromagnetic torque
T_L	load torque
J	rotor inertia constant
B_m	friction damping coefficient
ψ_m	magnet flux linkage
Vb	dc bus voltage for the inverter

Chapter 1

Introduction

1. 1. Background

If the Ancient Egyptian Faros or Romans, with their advanced civilization and knowledge of the sciences, had been able to develop a motor the course of history would have been much different. The development of the electric motor in modern times has indicated the truth in this theory. The development of the electric motor has given us the most efficient and effective means to do work known to man. The electric motor/generator is a simple device in principle. It converts electrical energy into mechanical energy in the case of motor and it converts mechanical energy in to electrical energy in the case of generator. Over the years, electric motors have changed substantially in design; however the basic principles have remained the same. The first generators and motors were called dynamos or dynamoelectric machines. Dynamo is from the Greek word dynamis which means power. Webster defines dynamoelectric as "relating to the conversion of mechanical energy into electrical energy or vice versa". The dynamo was the result of several people's relentless effort, in different countries and time, around the mid-nineteenth century [1]. Electromagnetism was discovered in 1822 by, a Danish scientist Hans Christian Oersted. In 1827 the law of electric conduction, known as Ohm's law was introduced by George S. Ohm, German and in 1830-31 electromagnetic induction was discovered first by Joseph Henry American, and later by Michael Faraday English [1,2]. Until recently, most motion control

systems were designed to operate at a fixed speed. Many existing systems still operate based on a speed determined by the frequency of the power grid. However, the most efficient operating speed for many applications, such as fans, blowers and centrifugal pumps, is different from the one that is enforced by the grid frequency and still to this day many high performance applications, such as robots, machine tools and the hybrid vehicle, require variable speed operation to begin with [1]. As a result, the transition from single speed drives to variable speed drives has been in effect since the 1970s mostly due to soaring energy cost and movements towards conservation of energy and protection of the environment. In particular, problems related to the efficiency of motors have received much attention due to their greater energy consumption and wide spread application in the industry [2]. About fifty eight percent of all electrical energy is, converted into mechanical energy, consumed by motors [2]. This may be the most important factor behind today's high demand for more efficient motion control systems. In general electric motors can be classified in to three major groups based on their working principle. Direct current (DC) motor, Induction motor (IM) and Synchronous motor [1, 2].

1. 2. DC Motor

By the early 1870s the Belgian-born electrical engineer Zénobe-Théophile Gramme had developed the first commercially viable dc motor. The name dc motor comes from the dc electric power used to supply the motor. The dc motor was in wide spread use in street railways, mining and industrial applications by the year 1900[2].The concept of controlled delivery of energy from a dc power source to a motor in order to meet the specific demands

of an application is emerged around the same year. The same technique is used today in the majority of high performance

control systems. However, the disadvantage of dc motors such as excessive wear in the electro-mechanical commutator, low efficiency, fire hazards due to sparking, limited speed and the extra room requirement to house the commutator, high cost of maintenance, became evident and leads to further investigation in order to overcome these dc motor disadvantages[1-3]. Michael Faraday's discovery of the electromagnetic induction concept in 1831 paved the way towards the invention of IM. After careful study of this electromagnetic theory a Serbian-American engineer Nikola Tesla invented the first alternating current, IM [1, 2]. By the year 1900 the principles of operation of synchronous and induction motors were well known, but they were not widely used at that time due to the fact that alternating current (AC) power was not yet commercially available. AC power is easier to produce, distribute, and utilize, as compared to dc power [2-4]. This flexibility of ac power led to its initial commercial success even if dc power still cost less at that time. Even though, the decoupled nature of the field and armature magneto motive force (MMF) makes DC motor very easy to control its torque and speed in a very precise manner, it has many disadvantages such as high cost, frequent need of maintenance, narrow speed range, etc.[4]. As a result the fierce competition between AC and DC power was finally resolved in favor of the AC power in 1890. AC motors have no commutator therefore there is no need for frequent maintenance, no need for housing the commutator, they have rugged construction and they have speed which is only limited by the physical constraints of the motor and the supply frequency. Wide spread utilization of ac motors in motion control applications was caused by these flexibilities [5].

1. 3. AC Motor

Most AC motors being used today are not synchronous motors. Instead, so-called "induction" motors which are the workhorses of the industry. So how is an IM different? The big difference is the manner in which current is supplied to the rotor [5]. There is no external power supply for the rotor instead the principle of induction technique is used. In an induction motor the current flow in the rotor is not caused by any direct connection of the conductors to a voltage source, but rather by the influence of the rotor conductors cutting across the lines of flux produced by the stator magnetic fields. The IM is a rotating electric machine designed to operate from a three-phase source of alternating voltage. The stator is a classic three phase stator with the winding displaced by 120° from each other. The most common type of induction motor has a squirrel cage rotor in which aluminum conductors or bars are shorted together at both ends of the rotor by cast aluminum end rings. When three currents flow through the three symmetrically placed stator windings, a sinusoidally distributed air gap flux generating rotor current is produced. The interaction of the rotating and sinusoidally distributed stator air gap flux and the flux generated by induced rotor currents produces a rotation. The rotor is connected to the motor shaft, so the shaft will also rotate and drive the load. The mechanical angular velocity of the rotor is always lower than the angular velocity of the flux wave by the so called slip velocity. The main advantages of induction motors are its lower cost, its maintenance free operation and its greater reliability especially in harsh industrial environments [5, 6]. On the contrary, induction motors require very complex control scheme because of their nonlinear relationship between the torque generating and magnetizing currents. In today world, most of the electric energy in the world is consumed by electric machines therefore the need for more energy efficient high

performance motor drive becomes the key factor in the advancement of electric machines. Recent developments in power electronics and microprocessors led to a revolutionary advancement in the design and control technique of electric machines. As a result, new machines such as synchronous motor emerged very recently.

1.4 Synchronous Motor

Synchronous motors utilize the same type of stator winding structure as IM and which is either a wound dc field or permanent magnet rotor. Synchronous motors run and generate torque at the synchronous speed which is the same as the source frequency. On the other hand, IM run and generate torque in a wide range of speed including zero speed. Therefore, prior to 1950 the speed of synchronous motors has to first be increased to synchronous speed by means of an auxiliary motor before the motor can be used [6]. In 1950 as an alternative to the auxiliary motor, a line-start PMSM which has a rotor made up of permanent magnet embedded inside a squirrel-cage winding is introduced. A line start PMSM starts as an induction motor and when the rotor speed reaches the synchronous speed it gets synchronized and rotate at synchronous speed. However, the advancement of power electronics and the introduction of high performance motor drives have rendered the line start PMSM almost obsolete because electronic converters can deliver appropriate power to synchronous motors so that they can start from zero speed by themselves as of IM [7].

1.5 Classification of Synchronous Motors

Beside conventional old wound rotor synchronous motor; based on the rotor structure synchronous motors can further be classified as (a) surface mounted permanent magnet synchronous motor (SMPMSM), (b) an inset or interior permanent magnet synchronous motor (IPMSM) and (c) reluctance synchronous motor (SyncRM) [8].

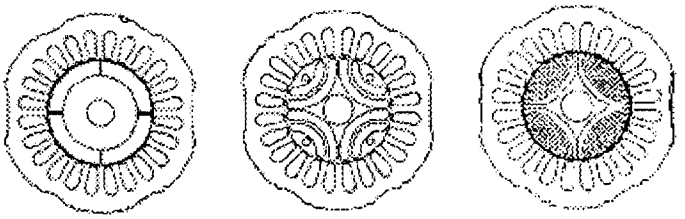

(a) (b) (c)

Fig.1 Show the cross-section of (a) SMPMSM, (b) IPMSM and (c) SyncRM rotor configuration.

1.5.1 SMPMSM

Fig.1. (a), shows arc-shaped permanent magnets mounted on the surface of a cylindrical rotor core to get a smaller uniform air gap. On the other hand, to prevent those magnets from detaching under the centrifugal force of rotation, they are covered by a thin cylindrical stainless steel can from the outside of the rotor. SMPMSM does not have magnetic saliency ($L_q = L_d$) therefore it can only utilize the developed magnetic torque.

Although it has a simple construction, the motor suffers from huge eddy current losses. Eddy current loss occurs on the surface of the stainless steel can that is attached to the outside of the rotor [8-10].

1.5.2 IPMSM

Fig.1. (b), shows the cross-section of an IPMSM constructed with permanent magnets embedded in the rotor core. IPMSM has a salient pole ($Lq > L_d$) because of that both magnetic and reluctance torque can be utilized in IPMSM drive and it is found to the most efficient all motors [8].

1.5.3 SyncRM

Fig.1 (c) shows a SyncRM which is not a permanent magnet rotor motor and it does not need any magnets. SyncRM has higher saliency ratio ($L_q < L_d$) by making the flux barrier slits on the rotor and it generate the reluctance torque derived from the difference in d-axis and q-axis inductance and suffers from higher degree of torque pulsation however, it is the cheapest among all synchronous motors [8-10].

Permanent magnet synchronous (PMSM) motors have found widespread applications in variable speed drives because of their various advantages such as high efficiency, high power density, high power factor, noise free operation and fast dynamics responses [9]. Fortunately, PMSM have additional advantage of working under a wide range of existing motor control schemes, such as vector control, maximum torque per ampere control, loss minimization control and power factor control etc. [9, 10]. This is mainly due to their inherent flexibility stem out from their rotor structures and magnets allocation inside the rotor

core [9-11]. The use of a permanent magnet to generate a substantial air gap magnetic flux makes it possible to design highly efficient PM motors. Usually, a PM Synchronous motor is driven by sine wave voltage coupled with the given rotor position. The generated stator flux in conjunction with the rotor flux defines the torque, and speed of the motor. A three phase supply voltage have to be applied to the 3-phase winding system in a way that the angle between the stator flux and the rotor flux is kept close to 90° to get the maximum generated torque. To meet this criterion, the motor drive requires electronic control for its proper operation.

1. 6 Thesis Objectives

As the above discussion depict, IPMSM possesses many appealing characteristics, such as high torque to inertia ratio, power to weight ratio plus low noise operation. However, due to the nonlinear nature of IPMSM both the magnitude and the angles of the current vectors need to be controlled. For this reason, the traditional scalar control is not suitable for high performance drive applications of IPMSM rather vector control technique will be an appropriate choice. Vector control scheme is used in the proposed efficiency optimization algorithm for speed control of IPMSM drive to decouple the torque and flux generating currents. As a result of decoupled torque and flux generating currents a faster and smooth transient and error free steady state response can be achieved. Over the past few years, awareness of environmental problems has grown dramatically worldwide, and tremendous interest has grown in developing energy efficient motor drives for the industry in order to address the environmental problem. The operating efficiency of a motor drive can be improved in many ways such as optimum rotor structure design and intervening in the motor

operation principle with different control techniques. Therefore, the objective of this thesis will be to develop an efficiency optimization algorithm based on the motor model and intervening in the drive control technique. As a result the developed algorithm improves the efficiency of the existing or newly implemented IPMSM drives at list by 4%. The developed efficiency optimization algorithm is as fast as the widely used vector control technique and is ideal for systems which need a rapidly changing steady state operation such as electric vehicles. It is almost impossible to a optimize a system operating in a rapidly changing steady state mode by using only an online efficiency optimization technique because the online optimizer needs to be turned off during transition until the system reached it steady state operation. In addition to the above mentioned disadvantage the online optimization technique also suffers from a serious torque ripple therefore the model based efficiency optimization is a good choice for IPMSM drive than the online one. By utilizing both the magnetic and reluctance torque of the IPMSM it is possible to calculate its core resistance R_c, and augmented it in to the IPMSM model and then develop a robust and fast vector controlled efficiency optimization control algorithm for speed control of an IPMSM.

1. 7 Thesis Outline

The organization of the remaining chapters is as follows. In Chapter 2, coordinate transformation and derivation of the mathematical model of IPMSM without the losses model is discussed. Here it is shown that how the vector control technique greatly simplifies the control of IPMSM. And then, the design of proportional integral (PI) speed controller based on the motor model equations, working principles of different PWM signal generators

where especial focus is paid to the hysteresis PWM signal generator and a voltage source inverter are discussed in detail with some illustrative diagrams. In chapter 3, background on efficiency optimization is laid in sections 3.1 and 3.2. In section 3.3 principles of energy optimization is discussed with some illustration. The mathematical model for the proposed efficiency optimization algorithm is also derived. In the last section of chapter 3 sample simulation results are presented and discussed. Then the complete IPMSM drive incorporating the electrical losses is presented. In Chapter 4 the real time implementation procedure for the complete drive system and the sample experimental results are presented and discussed. Finally, a summary of this work and suggestions for future work are highlighted in Chapter 5. After that, all pertinent references and appendices are listed.

Chapter 2

Mathematical Model of IPMSM without the Loss Model

In order to utilize the less complex linear behavior of the electrical system the following assumptions are taken before the IPMSM model is developed: (a) hysteretic loss, eddy current loss and magnetic saturation are neglected; (b) balanced three phase stator windings are assumed [12].

2.1 Coordinate transformation

If Ψ_m is the constant flux linkage provided by the permanent magnets(PM), then the flux linkages in the three phase stator winding due to PM of the rotor can be given as[10-13],

$$\begin{bmatrix}\Psi_{am}\\ \Psi_{bm}\\ \Psi_{cm}\end{bmatrix} = \Psi_m \begin{bmatrix}\sin\theta_r\\ \sin(\theta_r - \frac{2\pi}{3})\\ \sin(\theta_r + \frac{2\pi}{3})\end{bmatrix} \tag{2.1}$$

Where, Ψ_{am}, Ψ_{bm} and Ψ_{cm} are the three flux linkages of the three phase stator winding due to PM of the rotor and θ_r is the rotor position. The total air gap flux linkage of the three phases is the summation of the flux linkages due to the self inductance of the corresponding phase current, the mutual flux linkages due to currents in the other phases and the flux linkages in the three phase stator winding due to PM of the rotor. The air gap flux linkages of the three phases are given as,

$$\begin{bmatrix}\Psi_a\\ \Psi_b\\ \Psi_c\end{bmatrix} = \begin{bmatrix}L_{aa} & M_{ab} & M_{ac}\\ M_{ba} & L_{bb} & M_{bc}\\ M_{ca} & M_{cb} & L_{cc}\end{bmatrix}\begin{bmatrix}i_a\\ i_b\\ i_c\end{bmatrix} + \Psi_m \begin{bmatrix}\sin\theta_r\\ \sin(\theta_r - \frac{2\pi}{3})\\ \sin(\theta_r + \frac{2\pi}{3})\end{bmatrix} \tag{2.2}$$

Where, Ψ_a, Ψ_b and Ψ_c are the air gap flux linkages; L_{aa}, L_{bb}, L_{cc} are the self inductances and M_{ab}, M_{ac}, M_{ba} , M_{bc} , M_{ca} , and M_{cb} are the mutual inductances, of phase a, b, and c, respectively. The phase voltage is the voltage drop in each phase plus the voltages due to the rate of change of flux linkages. The three phase voltages which are the sum of the voltage drops and the induced voltages in each phase of the IPMSM can be described as:

$$v_a = r_a i_a + \frac{d\psi_a}{dt} \tag{2.3}$$

$$v_b = r_b i_b + \frac{d\psi_b}{dt} \tag{2.4}$$

$$v_c = r_c i_c + \frac{d\psi_c}{dt} \tag{2.5}$$

Where, v_a, v_b and v_c are the three phase voltages, i_a, i_b and i_c are the three phase currents and r_a, r_b and r_c are the three phase stator winding resistances. The above voltage equations can be written in compact form as follows:

$$\begin{bmatrix} v_a \\ v_b \\ v_c \end{bmatrix} = \begin{bmatrix} r_a & 0 & 0 \\ 0 & r_b & 0 \\ 0 & 0 & r_c \end{bmatrix} \begin{bmatrix} i_a \\ i_b \\ i_c \end{bmatrix} + \frac{d}{dt} \begin{bmatrix} \psi_a \\ \psi_b \\ \psi_c \end{bmatrix} \tag{2.6}$$

In order to alleviate the mathematical burden due to the none linear nature of the phase voltages v_a, v_b and v_c which are functions of the rotor position θ_r, which are dependent of the flux linkage components and have a time varying $(\frac{d}{dt})$ coefficient have to be transformed to the synchronously revolving rotor reference frame so that the machine equations become independent of the rotor position. These transformations can be accomplished in two steps [9]. First, v_a, v_b and v_c will be transformed from the stationary a-b-c frame into the stationary d-q frame and then from the stationary d-q frame to the synchronously rotating d^e-q^e excitation frame. The transformed phase variables in the stationary d-q-0 axis can be written in matrix form as:

$$\begin{bmatrix} v_a \\ v_b \\ v_c \end{bmatrix} = \frac{2}{3}\begin{bmatrix} \cos\theta_r & \sin\theta_r & \\ \cos(\theta_r - \frac{2\pi}{3}) & \sin(\theta_r - \frac{2\pi}{3}) & 1 \\ \cos(\theta_r + \frac{2\pi}{3}) & \sin(\theta_r + \frac{2\pi}{3}) & 1 \end{bmatrix}\begin{bmatrix} v_q \\ v_d \\ v_0 \end{bmatrix} \tag{2.7}$$

The corresponding inverse relation can be written as,

$$\begin{bmatrix} v_q \\ v_d \\ v_0 \end{bmatrix} = \frac{2}{3}\begin{bmatrix} \cos\theta_r & \cos(\theta_r - \frac{2\pi}{3}) & \cos(\theta_r + \frac{2\pi}{3}) \\ \sin\theta_r & \sin(\theta_r - \frac{2\pi}{3}) & \sin(\theta_r + \frac{2\pi}{3}) \\ \frac{1}{2} & \frac{1}{2} & \frac{1}{2} \end{bmatrix}\begin{bmatrix} v_a \\ v_b \\ v_c \end{bmatrix} \tag{2.8}$$

Whereas the rotor angle or rotor position is given by,

$$\theta_r = \int_0^t \omega_r(\tau)d\tau + \theta_r(0) \tag{2.9}$$

For a balanced three phase, zero-sequence component (v_0) does not exist, therefore it is convenient to set initial rotor position $\theta_r(0) = 0$ so that the q axis coincides with phase a. Under these condition (2.8) can be given as:

$$\begin{bmatrix} v_a \\ v_b \\ v_c \end{bmatrix} = \begin{bmatrix} 1 & 0 \\ -\frac{1}{2} & -\frac{\sqrt{3}}{2} \\ -\frac{1}{2} & \frac{\sqrt{3}}{2} \end{bmatrix}\begin{bmatrix} v_q \\ v_d \\ 0 \end{bmatrix} \tag{2.10}$$

and the inverse is given as:

$$\begin{bmatrix} v_q \\ v_d \\ 0 \end{bmatrix} = \begin{bmatrix} \frac{2}{3} & -\frac{1}{3} & -\frac{1}{3} \\ 0 & -\frac{1}{\sqrt{3}} & \frac{1}{\sqrt{3}} \end{bmatrix}\begin{bmatrix} v_a \\ v_b \\ v_c \end{bmatrix} \tag{2.11}$$

Variables in the stationary d-q frame can be transformed to the synchronously rotating $d^e - q^e$ excitation frame as follow:

$$\begin{bmatrix} d_q^e \\ d_d^e \end{bmatrix} = \begin{bmatrix} \cos\theta_r & -\sin\theta_r \\ \sin\theta_r & \cos\theta_r \end{bmatrix} \begin{bmatrix} d_q \\ d_d \end{bmatrix} \tag{2.12}$$

and the inverse relation can be given as:

$$\begin{bmatrix} d_q \\ d_d \end{bmatrix} = \begin{bmatrix} \cos\theta_r & \sin\theta_r \\ -\sin\theta_r & \cos\theta_r \end{bmatrix} \begin{bmatrix} d_q^e \\ d_d^e \end{bmatrix} \tag{2.13}$$

In the above equation the motor voltage is taken in to consideration but all transformation equations are equally valid for the motor current as well as flux. Assuming, negligible eddy current, hysteresis and copper losses, sinusoidal back emf, balanced three phase winding and a negligible magnetic saturation; the $d^e - q^e$ axis of IPMSM model can be given as follows,

$$v_q^e = Ri_q^e + \frac{d\psi_q^e}{dt} + \omega_s \psi_d^e \tag{2.14}$$

$$v_d^e = Ri_d^e + \frac{d\psi_d^e}{dt} - \omega_s \psi_q^e \tag{2.15}$$

Where, v_q^e , v_d^e , i_q^e , i_d^e and ψ_q^e , ψ_d^e are q-d axis voltage, current and axis flux linkages respectively. R is the stator resistance per phase and ω_s is the stator frequency. Further, ψ_q^e , ψ_d^e can be expressed as:

$$\psi_q^e = L_q i_q^e \tag{2.16}$$

$$\psi_d^e = L_d i_d^e \tag{2.17}$$

Where, $L_q = L_l + L_{mq}$

$L_d = L_l + L_{md}$

Where, L_d and L_q are d-q axis inductances, L_{md}, L_{mq} are d-q axis magnetizing inductances, respectively and L_l is the leakage inductance per phase. The rotor frequency ω_r, is related to the stator frequency (ω_s) as shown in (2.18).

$$\omega_s = P\omega_r \tag{2.18}$$

Where, P is the number of poles in the motor.

Using equations (2.14)-(2.18), the mathematical motor model is given by (2.19),

$$\begin{bmatrix} v_q \\ v_d \end{bmatrix} = \begin{bmatrix} P\omega_r L_d & R_s + \frac{dL_d}{dt} \\ R_s + \frac{dL_d}{dt} & -P\omega_r L_q \end{bmatrix} \begin{bmatrix} i_q \\ i_d \end{bmatrix} + \begin{bmatrix} P\omega_r \psi_m \\ 0 \end{bmatrix} \tag{2.19}$$

Based on (2.16)-(2.19), the d-q axis equivalent circuit diagram can be constructed as shown in Fig.2.1.

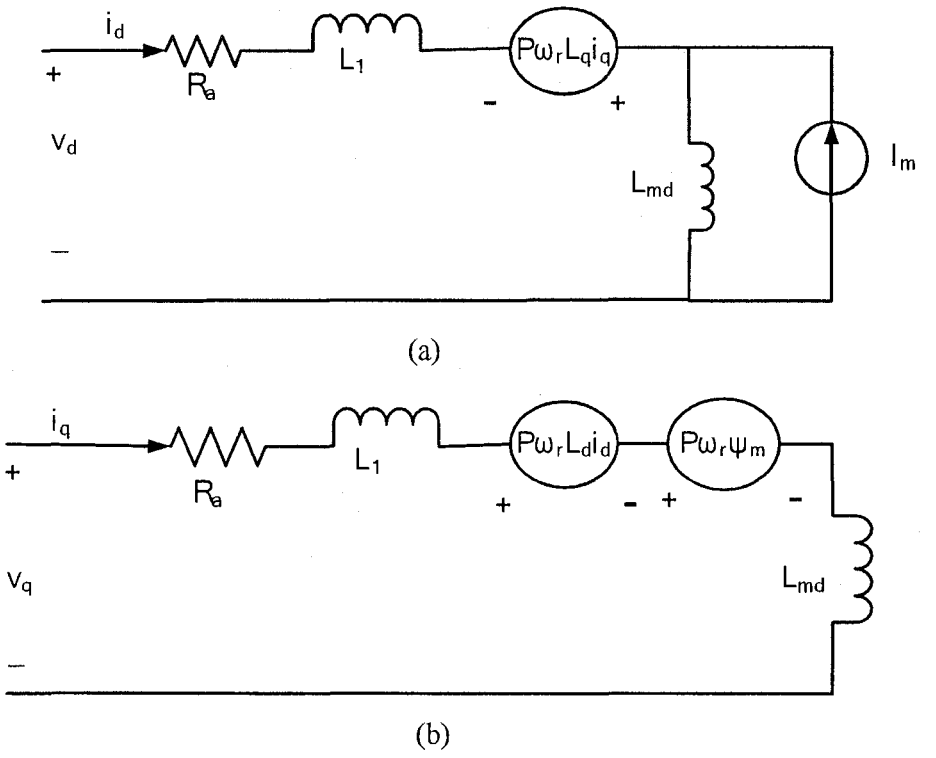

Fig.2.1 d-q axis equivalent circuit model of IPMSM; (a) d-axis and (b) q-axis.

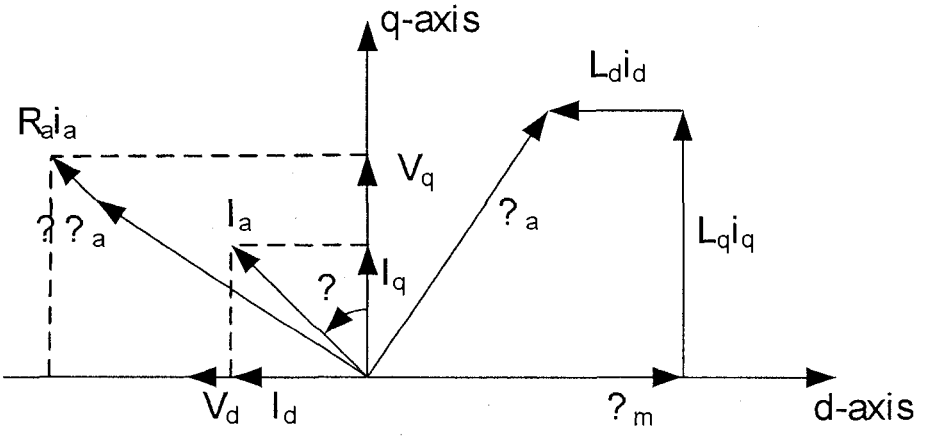

Fig.2.2 Basic phasor diagram of an IPMSM.

The steady state stator phase voltage V_a can be derived from the d-q equivalent circuit of IPMSM model as in (2.20). If the d- axis is taken as the reference phasor, then V_a can be calculated as follows [13].

$$V_a = \left[\left(R_a i_d - \omega L_q i_q\right)^2 + \left(R_a i_q + \omega\left(\psi_m + L_d i_d\right)\right)^2\right]^{0.5} \quad (2.20)$$

Where the stator phase current I_a is given by (2.21),

$$I_a = \left(i_d^2 + i_q^2\right)^{0.5} \quad (2.21)$$

The stator current can be controlled by controlling the individual d-q current components. When i_d is set to zero, i_a is a function of of i_q, and hence can be controlled by controlling i_q. Thus, constant output torque can be found by keeping i_q constant. The total average power per phase supplied by the source in the excitation frame is calculated as (2.22). This input power is the same as the developed power because the magnetic saturation, the eddy current, the hysteresis and the copper losses are assumed negligible [4, 5, and 12].

$$p_{phase} = \frac{1}{2}\left(-P\omega_r L_q i_q^e i_d^e + P\omega_r L_d i_q^e i_d^e + P\omega_r \psi_m i_q^e\right) \quad (2.22)$$

And the total power developed by the machine is given by (2.23),

$$p_{total} = \frac{3}{2} P\omega_r\left(\psi_m i_q^e + (L_d - L_q) i_q^e i_d^e\right) \quad (2.23)$$

The average torque T_e developed by the IPMSM is derived from the d-q axis equivalent circuit of Fig.2.1 and shown as:

$$T_e = \frac{P_{mech}}{\omega_r} = \frac{3P}{2}\left(\psi_m i_q^e + (L_d - L_q) i_q^e i_d^e\right) \tag{2.24}$$

The two terms in this equation reflects an important aspect of the torque production in an IPMSM. First, the magnet flux oriented along the rotor d-axis interacts with the q-axis stator current to produce a field-alignment torque proportional to the (ψ_m I_q) This is the same process by which torque is produced in a conventional SMPMSM. In addition, the current-induced magnetic fluxes along the two axes $L_d i_d$ and $L_q i_q$ interact with the orthogonal current components to contribute a second torque term. The rotor saliency is clearly responsible for the presence of this reluctance torque term, which is proportional to the axis inductance difference (L_d - L_q). Thus the torque equation suggests that, for the purposes of conceptualization, the IPMSM can be considered as a combination of the SynRM and SMPMSM machines and the dynamic model is given as (2.25).

$$T_e = T_L + B_m \omega_r + J\frac{d\omega_r}{dt} \tag{2.25}$$

Where T_L is the load torque in Nm, B_m is the friction damping coefficient in Nm/rad/sec and J is rotor inertia constant in kg-m^2.

2.2. Vector Control scheme for IPMSM Drive

The objective of vector control is to eliminate the coupling between the direct and quadrature axes currents by doing so both the phase angle and the magnitude of the current can be controlled. Park's theory presented a frame transformation between variables in the stationary reference frame and the rotor reference frames which yields a two-axis equivalent circuit for PMSM. After Park's transformation every variable will have a magnitude and angle which is constant in steady state from the rotor's point of view and this transformation alleviates the mathematical burden of the drive. The torque versus current relationship of synchronous motor is non-linear [10-12]. The torque of synchronous motor depends on both current magnitude and phasor angle with respect to the rotor. This results in complication as far as the motor control is concerned. Availability of Park's transformation led to a technique referred to as vector control. Vector control enables independent control over the magnitude and the phase angle between the current phasor and the rotor flux vector such that instantaneous control over torque is possible.

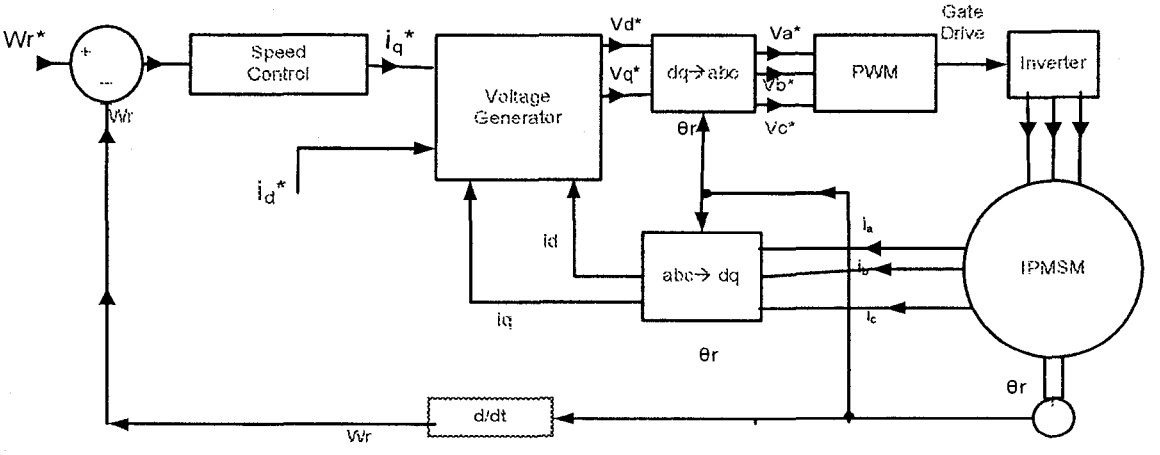

Fig.2.3 Vector control of electric motors.

Fast and accurate response and quick recovery of speed from any disturbances are some of the important characteristics of high performance drives. Because, vector control technique possesses these characteristics it becomes the favourable choice of the industry for variable speed motor drives. In vector control, first the machine equations are transformed from three phase to two phase stationary reference frame by utilizing Clark's transformation equation as given by (2.10). Clark's transformation shows that any three phase rotating vector system can be decomposed in to an equivalent two phase orthogonal system, called direct and quadrature axis. It is commonly expressed with the direct axis aligned with the stator axis. Then the machine equation in the two phase stator stationary frame will be transformed to a synchronously rotating excitation frame by using Park's transformation as shown in (2.12). This transformation is linear and reversible. Second, i_d^e in (2.24) is set to zero in order to eliminate the second term of the torque equation which results in a linear relationship between the developed torque and the torque generating current i_q^e as shown in (2.26).

$$T_e = \frac{3}{2} P \psi_m i_q^e \tag{2.26}$$

The instantaneous torque of IPMSM is the vector product of the air gap flux linkage vector and the torque component current vector which is orthogonal to the flux vector. The torque component current vector and flux component current vector are decomposed from the current vector of the IPMSM by using the park's transformation and are controlled independently where the flux component current vector is parallel to the air gap flux linkage vector. If the amplitude of the air gap flux linkage is kept constant, the machine torque is controlled instantaneously by the amplitude of the torque component current vector.

Therefore the IPMSM controlled by the vector control scheme becomes as easy as controlling a separately excited dc machine.

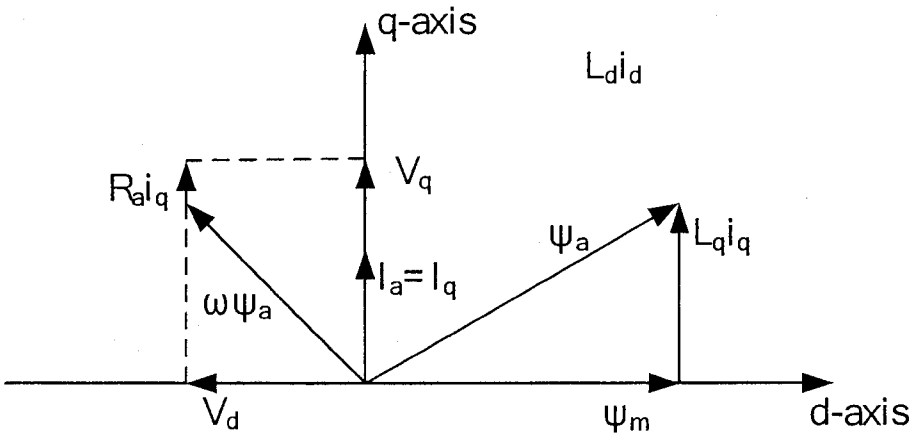

Fig 2.4 Phasor diagram of a IPMSM with $i_d = 0$.

In this control technique the current phase angle $\square = 0^0$ and it is the most efficient angle for a SMPMSM. The motor is driven at this phase angle and for this control technique; the dynamic equations (2.27) to (2.29) can be rewritten as,

$$i_q = \frac{-R_a i_q^e - P\omega_r \psi_m + v_q^e}{L_q} \tag{2.27}$$

$$v_d^e = -P\omega_r L_q i_q^e \tag{2.28}$$

$$\frac{d\omega_r}{dt} = \frac{T_e - T_L - B_m \omega_r}{J} \tag{2.29}$$

Notice that all the voltages and currents in (2.27-2.28) are in the excitation frame. For this thesis a complete closed loop vector control technique is chosen and implemented using a hysteresis current controller in the proposed efficiency optimization algorithm for speed control of IPMSM.

2.3. The Speed controller

Speed control is essential for a high performance drive application; since a motor must have a fast, accurate speed tracking response and quick recovery of speed from any disturbances for such applications like rolling mills, machine tools, etc. Since the major focus of this work is to develop a generalized energy optimization algorithm for IPMSM drive, the conventional proportional integral (PI) controller is chosen because of its simplicity and most of all because of its faster response despite of its pronounced sensitivity and fixed gain. However, any kind of suitable controller can be used for example; if their sluggish response is easily compensated fuzzy logic or neural network fuzzy logic controllers are good candidates for consideration because of their better ability to handle nonlinearity, such as parameter variations due to temperature rise in the case of IPMSM and etc. [15]. The PI controller has speed error as its input and i_q^* as its output. The PI speed controller is given by (2.28).

$$i_q^* = K_p \Delta\omega_r + K_i \int \Delta\omega_r dt \tag{2.28}$$

$$\Delta\omega_r = \omega - \omega r \tag{2.29}$$

Where K_p is the proportional gain and K_i is the integral gain and $\Delta\omega_s$ is speed error. The PI controller is tuned by trial and error as a result proportional gain K_p and integral gain K_i found to be 10 and17 respectively.

2.4. Pulse Width Modulation (PWM)

PWM signals are pulse trains with fixed frequency and magnitude and variable pulse width [15, 16]. There is one pulse of fixed magnitude in every PWM period. However, the width of the pulses changes from period to period according to a modulating signal. When a PWM signal is applied to the gate of a power transistor, it causes the turn-on and turn-off intervals of the transistor to change from one PWM period to another PWM period according to the same modulating signal. The frequency of a PWM signal must be much higher than that of the modulating signal, the fundamental frequency, such that the energy delivered to the motor and its load depends mostly on the modulating signal. Figure 6 shows two types of PWM signals, symmetric and asymmetric edge-aligned. The pulses of a symmetric PWM signal are always symmetric with respect to the center of each PWM period. The pulses of an asymmetric edge-aligned PWM signal always have the same side aligned with one end of each PWM period.

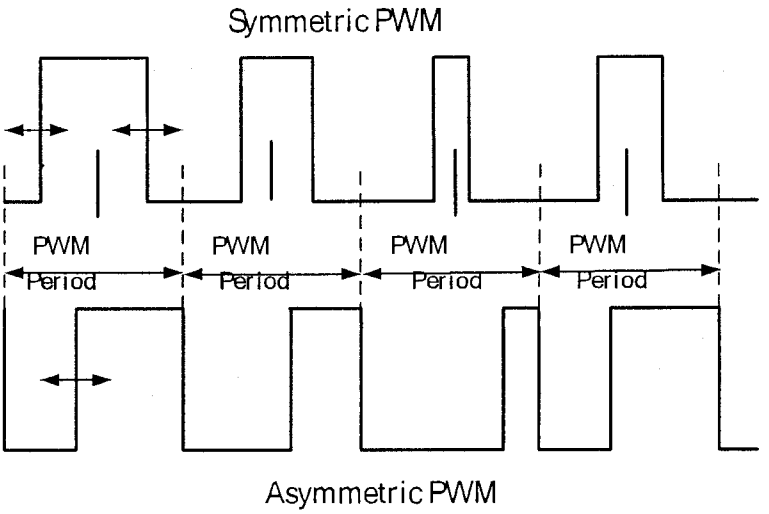

Fig.2.5 Symmetric and asymmetric PWM signals.

Both types of PWM signals can be used for motor drive application however; the symmetric PWM signals have the advantage of generating fewer harmonic in the output currents and voltages [17]. Different PWM techniques, or ways of determining the modulating signal and the switch-on/switch-off instants from the modulating signal, exist. The most common examples are sinusoidal PWM, hysteresis PWM and the relatively new space vector PWM. These techniques are commonly used with three phase voltage source power inverters and supply three-phase motors. The hysteresis PWM technique is employed in this thesis and will be discussed in more details. Carrier based PWM with a sinusoidal/triangle wave modulation signal is one of the earliest and widely used techniques for most variable drive applications. In carrier based PWM, three phase reference modulating signals are compared against a common sinusoidal/triangular carrier wave to generate the PWM signals. Carrier-Based PWM is comprised of Modulation signal and carrier signal and it is divided in to two mode of operation. The linear mode, when the amplitude modulation index (M< or =1), and non-linear

mode of operation when (M>1) resulting in no intersection point between the carrier signal and modulating signal. Where, M the frequency modulation index is defined as the ratio of carrier frequency over the modulating signal frequency. Carrier-Based PWM maintain good performance of the drive in the entire range of operation between 0%-100% modulation indexes M. If the modulation index exceeds this range then an optimized PWM with pre calculated switching point and stored in the look up table is required. The use of higher switching frequency produces a nearly sinusoidal fundamental voltage output. At lower frequency this results in smooth speed and torque performance and freedom from cogging dawn at zero speed at reversal of direction of rotation.

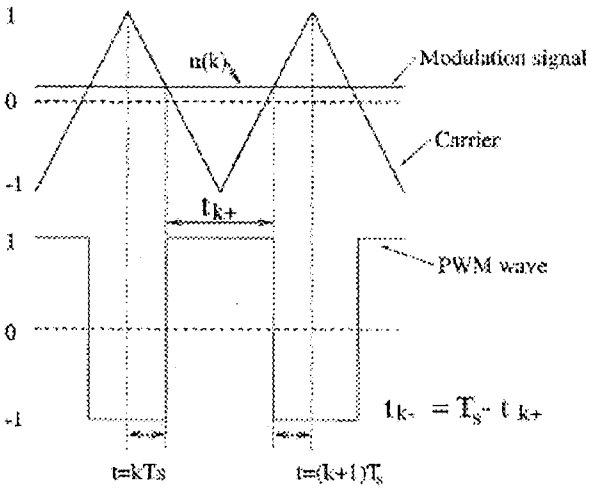

Fig.2.6 Two level carrier based-PWM.

$$u_k T_s = t_{k+} - t_{k-} \tag{2.30}$$

$$t_{k+} = \frac{1}{2}(1 + u_k)T_s \tag{2.31}$$

$$t_{k-} = \frac{1}{2}(1 - u_k)T_s \tag{2.32}$$

In Fig.2.6 linear mode carrier based PWM two level modulator the on and off switching time can be calculated as (2.30-32).Where T_s , t_{k+} and t_{k-} are the sampling time, the

positive and negative pulse widths in the k_{th} sampling intervals, respectively. Whereas, M_a is the normalized peak value of the carrier signal and it will have a maximum value of 1. This equation is referred to as the equal voltage -second principle [15].

2.5. Hysteresis current controller

Hysteresis current control is one of the most effective and simple control methods [10].

A single phase hysteresis current controller is shown in Fig.2.7.

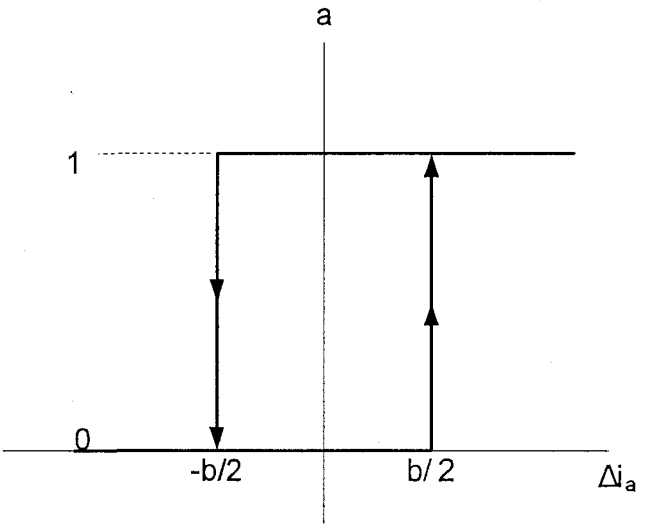

Fig.2.7 Input-output characteristic of hysteresis current controller.

The hysteresis controller presented in Fig.2.7 has a sensitivity or tolerance band width designated by b. This band width prevents the outputs of the hysteresis current control from switching between 1 and 0 each time Δi crosses zero unless and otherwise it exceeds the specified magnitude of b. As illustrated in Fig.2.6 if the current Δi_a exceeds b/2 then the hysteresis current controller output will be set to 1; on the contrary, if the current Δi_a below -b/2 the hysteresis current controller output will be set to 0. However, if the value of Δi_a remains in between $\frac{-b}{2}$ and $\frac{b}{2}$ then the hysteresis current controller retains its previous output

value unchanged. It is obvious to see that the narrower the hysteresis band the higher the inverter's switching frequency becomes and the inverter quality improves as a result.

2.6. Inverter

For adjustable speed drive applications, AC motors are powered by inverters because of advances in solid state power devices and microprocessors. The inverter converts DC power to AC power as well as offer an easy way to regulate both the frequency and magnitude of the voltage and current applied to a motor [17]. As a result much higher efficiency and performance can be achieved by these motor drives with less generated noises [18].

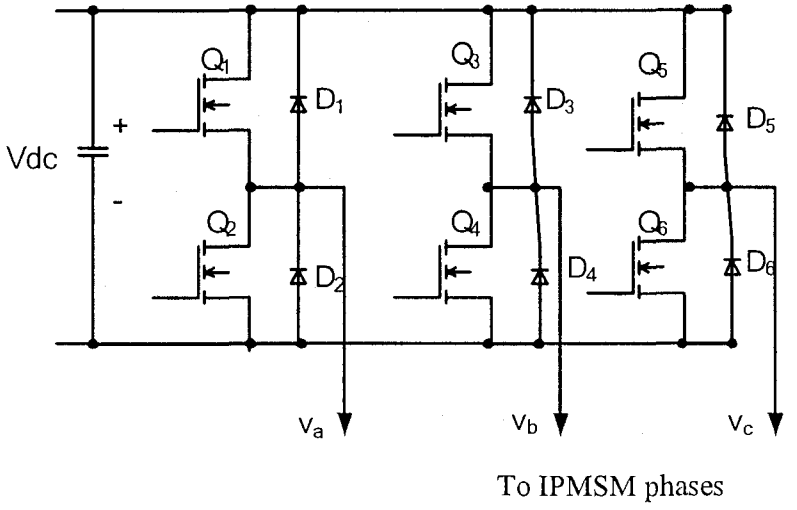

Fig.2.8 Three half-bridge inverter.

As shown in the diagram, the inverter consists of three half-bridge units, each made up of two transistors and two freewheeling diodes, where the upper and lower switches are controlled

complimentarily. As the power device's turn-off time is longer than its turn-on time, some dead-time must be inserted between the turn-off of one transistor of the half-bridge and turn-on of its complementary device. The output stage a PWM inverter can be conceptually represented by the set of single-pole double through switches. Through the proper activation of the switches, the fixed dc link voltage is applied for short time interval with either polarity to the load terminals in such a way as to result in fundamental output voltage of adjustable magnitude and frequency. A voltage source inverter is commonly used to supply a variable frequency and variable voltage to a three phase motor in a variable speed application. A suitable pulse width modulation (PWM) technique is employed to obtain the required output voltage in the line side of the inverter [18, 19]. The power stage of a motor drive utilizes six power transistors with independent switching. The power transistors are switched in the complementary mode. The two transistors in the given branch for example, Q1 and Q2 are prohibited to be in ON or OFF position simultaneously or else the output of the corresponding terminal of the inverter cannot be determined. This implies that, in a given branch if one transistor must be in ON position and then the other must be kept at OFF position [13]. If two switching logic positions are assigned to each of the three branches of the inverter $(2^3 = 8)$ then eight possible switching positions are composed for the inverter output as shown in table (2.1).

Table 2.1: Conduction mode of current controlled voltage source inverter

State	Phase a A	Phase b B	Phase c C	Operating	Voltage

	Q_1	Q_2	Q_3	Q_4	Q_5	Q_6	mode	phasor
0	0	1	0	1	0	1	freewheeling	V_0
1	1	0	0	1	0	1	active	V_1
2	0	1	1	0	0	1	active	V_2
3	1	0	1	0	0	1	active	V_3
4	0	1	0	1	1	0	active	V_4
5	1	0	0	1	1	0	active	V_5
6	0	1	1	0	1	0	active	V_6
7	1	0	1	0	1	0	freewheeling	V_7

The switching position defined as;

$$A = 0 \text{ if } Q_1 \text{ is OFF and } Q_2 \text{ is ON}$$

$$1 \text{ if } Q_1 \text{ is ON and } Q_2 \text{ is OFF}$$

$$B = 0 \text{ if } Q_3 \text{ is OFF and } Q_4 \text{ is ON}$$

$$1 \text{ if } Q_3 \text{ is ON and } Q_4 \text{ is OFF}$$

$$C = 0 \text{ if } Q_5 \text{ is OFF and } Q_6 \text{ is ON}$$

$$1 \text{ if } Q_5 \text{ is ON and } Q_6 \text{ is OFF}$$

The line – to line voltages of the inverter are defined as follow;

$$v_a = \frac{v_{DC}}{3}(2A - B - C) \tag{2.33}$$

$$v_b = \frac{v_{DC}}{3}(2B - C - A) \tag{2.34}$$

$$v_c = \frac{V_{DC}}{3}(2C - A - B) \tag{2.35}$$

The above equations indicated that the line to line voltages can assume any one of five values at each switching positions as shown in (2.36).

$$\frac{-2}{3}V_{dc}, \frac{-1}{3}V_{dc}, 0, \frac{1}{3}V_{dc}, \frac{2}{3}V_{dc} \tag{2.36}$$

By utilizing Clark's three phases to two phase transformation given by (2.11) the output voltages can be represented as space vector in stator reference frame where each vector matches to a given switching position of the inverter. The space vector diagram of the line to line output voltages of an inverter is illustrated in Fig 2.8.

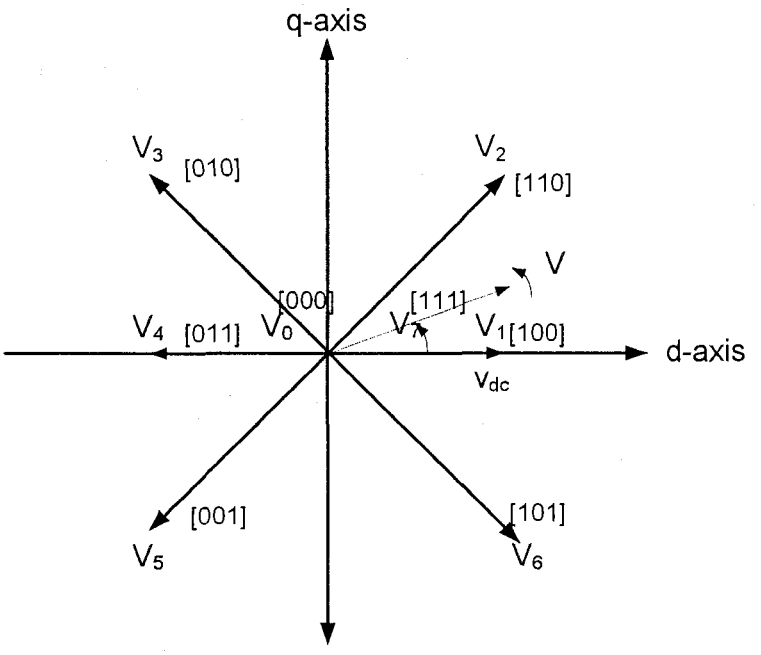

Fig.2.8 Space vector diagram for the line to line output voltage of an inverter.

The energy that an inverter delivers to a motor is controlled by Pulse Width Modulated (PWM) signals applied to the gates of the power transistors. And a voltage source inverter is commonly used to supply a variable frequency and variable voltage to a three phase motor in a variable speed drive application [17-19]. A three phase hysteresis current control fed voltage source inverter is shown in Fig. 2.9.

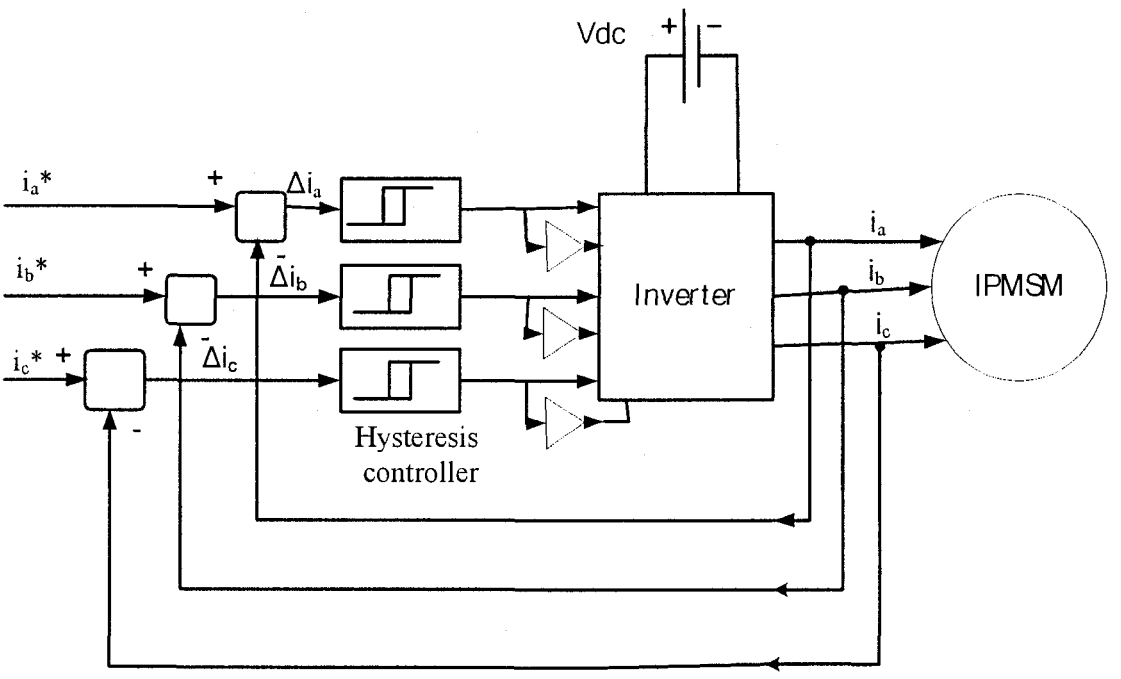

Fig. 2.9 Block diagram of current controlled voltage source inverter.

Current error signals Δi_a, Δi_b and Δi_c are generated by comparing i_a, i_b and i_c the inverter's output currents and the command currents i_a*, i_b* and i_c*. Then, Δi_a, Δi_b and Δi_c are fed to the hysteresis current controller in order to produce the PWM signal that triggers the inverter gates. Then in accordance to the PWM signal, the power transistors in the inverter apply V_{dc} for short period of time such that it results in a fundamental output voltage of adjustable magnitude and frequency to supply the IPMSM.

Chapter 3

3.1 Back ground on Efficiency Optimization of IPMSM Drive

There have been growing concerns over energy consumption and the environment, due to the soaring energy cost and tighter environment protection laws. With soaring energy costs and tighter environmental laws, increasing the efficiency of the electrical drive system is very important. In particular, concerns related to the efficiency of IPMSM have received much attention due to their growing application in the industrial field [1]-[3]. The IPMSM gains its popularity in variable speed drive applications because of its advantages such as high efficiency, high power density, high power factor low noise and robustness as compared to the conventional IM and other AC motors [20]. The IPMSM rotor is made up of permanent magnets buried in the rotor core; the rotor losses in the IPMSM are significantly lower than the IM, since no current-carrying conductor exists in the rotor to accumulate copper losses in the form heat. The reductions in the rotor losses are particularly valuable since heat are almost always more difficult to thermally extract from a spinning rotor than from the surrounding stator [20], [21]. The operating efficiency of a motor drive can be improved either through optimum rotor structure design or intervening in the motor operation principle with different control techniques or both. The optimum rotor structure design already exploited in IPMSM during utilization of reluctance torque yield from the d-q axis inductance value differences. On the other hand in an attempt to intervene in the motor

operation and improve the efficiency of IPMSM drive, several control methods have been proposed. [21]. For example, copper loss can be minimized by the maximum torque-per-ampere current control technique [20]. The power factor control method for efficiency improvement of IPMSM, keeping a unity power factor, is described in [22] however, the power factor of the IPMSM is maximized but still power losses are not minimized. Traditionally, the IPMSM has been controlled by keeping the d-axis component of the stator current, $i_d = 0$ in order to make the control task easier [22]. Nevertheless, with $i_d=0$ control it is not possible to control the air gap flux and hence the efficiency of the motor cannot be optimized [20]-[23]. In addition to that, with $i_d=0$ control the reluctance torque of IPMSM cannot be utilized, which is the advantageous feature of IPMSM as compared to a surface mounted permanent magnet synchronous motor. Especially, at light load condition the motor flux become excessive for the developed torque resulting in higher iron loss and poor efficiency of the motor [21,22]. The efficiency of IPMSM greatly improved by reducing the air gap flux because the iron loss is roughly proportional to square of the air gap flux density.

3.2 Types of efficiency optimization techniques

There are two major efficiency optimizing techniques for IPMSM such as, (a) Search based, and (b) model-based efficiency optimization techniques [24]. Both efficiency optimizing techniques have been used in vector-controlled IPMSM drives [24, 25]. The search based loss minimization technique has its own advantages such as insensitivity to parameter variations caused by temperature and magnetic saturation [20]. In this search based loss minimization technique the flux is decremented in steps wise manner until the lowest

value of the IPMSM losses, optimal operating point, is reached. However, there are outstanding disadvantages in the application of this technique. First, torque ripple appears each time the flux is stepped down to reach the optimal operating point [21]. Second, when the optimal operating point is found, electromagnetic torque reserve is so low that motor is very sensitive to load perturbations. Third, convergence of the magnetizing current toward the optimum value is very slow and wouldn't reach its optimal value but oscillates around it in small steps. Due to the above mentioned and other disadvantages the search based efficiency optimization technique is not utilized that much in the industry. On the other hand, model based efficiency optimization converges rapidly to its optimal operating point and does not produce torque ripple even though it is sensitive to parameter variation [24]. For these reasons model based efficiency optimization is chosen and implemented in this work.

3.3 Mathematical Model of IPMSM Including Motor Losses

The problem of core loss calculations in electrical motors is of interest for at least two reasons. First, it helps to evaluate the heat developed in the motor and the means needed to reduce and remove it. Secondly, motor control processes take more and more sophisticated forms with the advent of faster and more powerful power electronic components and microprocessors. An important requirement is to find an electric circuit which is equivalent to the electric motor and can adequately describe motor behaviour. Motor core losses determine one of the components in this equivalent circuit [25]. From the theoretical analysis, a condition that specifies the optimal d-axis component of the stator current for minimizing

IPMSM losses is derived. An equivalent d-q axis model of IPMSM with simplified loss model representation is shown in Fig.3.1

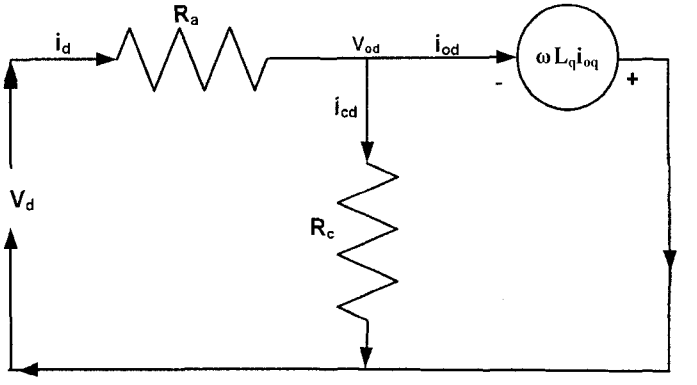

(a)

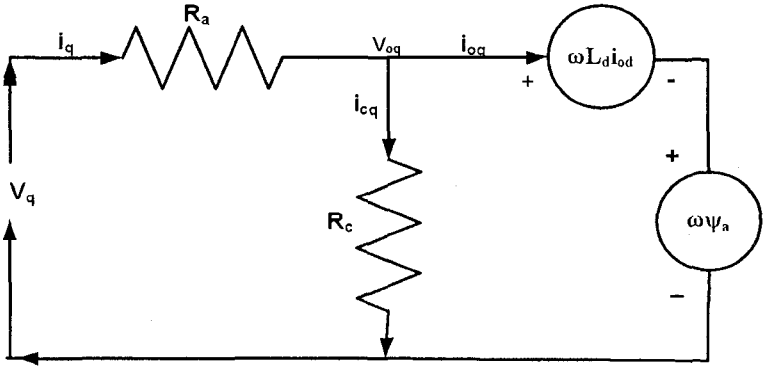

(b)

Fig.3.1 d- q axis model of IPMSM incorporating iron loss.

In Fig.3.1 d-q axis model of IPMSM; i_d and i_q are d-axis and q-axis stator currents, V_d and V_q are the d-axis and q-axis armature voltages, i_{od} and i_{oq} are the d-axis demagnetizing and q-axis torque generating operating point currents, i_{cd} and i_{cq} are d-axis and q-axis core loss currents, R_a and R_c represents the copper and core losses respectively. The harmonics in the

back EMF also generate an iron loss. However, this harmonic generated iron loss is not controllable therefore its effect is not considered in this thesis. L_q and L_d are q-axis and d-axis self inductances, respectively. Whereas ψ_a is magnet flux linkage, ω is the electrical speed and ω_r is the rotor speed. The following equations (3.1)-(3.5) are derived based on Fig.3.1.

$$\begin{bmatrix} V_d \\ V_q \end{bmatrix} = R_a \begin{bmatrix} i_{od} \\ i_{oq} \end{bmatrix} + \left(1 + \frac{R_a}{R_c}\right) \begin{bmatrix} V_{cd} \\ V_{cq} \end{bmatrix} \tag{3.1}$$

$$\begin{bmatrix} V_{od} \\ V_{oq} \end{bmatrix} = \begin{bmatrix} 0 & -\omega \rho L_q \\ \omega L_d & 0 \end{bmatrix} \begin{bmatrix} i_{od} \\ i_{oq} \end{bmatrix} + \begin{bmatrix} 0 \\ \omega \psi_a \end{bmatrix} \tag{3.2}$$

$$i_{od} = i_d - i_{cd} \tag{3.3}$$

$$i_{oq} = i_q - i_{cq} \tag{3.4}$$

$$i_{cd} = -\frac{\omega \rho i_{oq} L_d}{R_c} \tag{3.5}$$

$$i_{cq} = \frac{\omega(\psi_a + L_d i_{od})}{R_c} \tag{3.6}$$

The armature current I_a, the terminal voltage V_a and the developed average torque T_e are expressed in (3.6), (3.7) and (3.8) respectively.

$$I_s = \sqrt{(i_d^2 + i_q^2)} \tag{3.6}$$

$$V_s = \sqrt{[(R_s i_d - \omega \rho L_d i_{oq})^2 + (R_s i_q + \omega(\psi_a + L_d i_{od}))^2]} \tag{3.7}$$

$$T_e = P(\psi_a i_{oq} + (1-\rho) L_d i_{od} i_{oq}) \tag{3.8}$$

The developed torque can be modified in terms of the current phase angle as follows,

$$T_e = P(\psi_a i_a \cos\beta + \frac{1}{2}(\rho - 1) L_d i_a^2 \sin 2\beta) \tag{3.9}$$

Where, $\beta = \tan^{-1}\left(\frac{i_d}{i_q}\right)$ is the current phase angle, $\rho = \frac{L_q}{L_d}$, P is number of pole pairs, I_a is rms value of stator line current and V_a is rms value of stator line voltage. The first term in (3.8) represents the magnetic torque and the second term is the reluctance torque. Copper and core losses are the two controllable losses in IPMSM [26]. Core loss is the combined effect of eddy current and hysteresis losses. Eddy current losses are caused by the flow of induced currents inside the stator core and hysteresis losses are caused by the continuous variation of flux linkages and frequency of the flux variation in the core [26], [27]. Based on equations (3.3), (3.4) and Fig.3.1 the copper loss P_{Cu}, the iron loss P_{Fe} and the mechanical loss P_M can be expressed as,

$$P_{cu} = R_s(i_d^2 + i_q^2)$$

$$= R_s\left(\left(i_{od} - \frac{\omega \rho i_{oq} L_q}{R_s}\right)^2 + \left(i_{oq} + \frac{\omega(\psi_a + L_d i_{od})}{R_s}\right)^2\right) \tag{3.10}$$

$$P_{Fe} = R_c\left(i_{cd}^2 + i_{cq}^2\right)$$

$$= \left(\frac{(\omega p i_{sq} L_d)^2}{R_c}\right) + \left(\frac{\omega^2(\psi_a + L_d i_{sd})^2}{R_c}\right) \tag{3.11}$$

$$P_M = T_F \omega_r \tag{3.12}$$

Where T_F is the frictional torque of the motor and $\omega_r = (\omega/p)$ is the angular velocity of the motor where ω is the electrical speed. Unlike P_{cu} and P_{Fe}, the speed dependent P_M is not controllable by the efficiency optimization algorithm. The output power P_{out} and efficiency of the IPMSM drive η are expressed as,

$$P_E = P_{cu} + P_{Fe}$$

$$= R_a\left(i_{sd}^2 + i_{sq}^2\right) + R_c\left(i_{cd}^2 + i_{cq}^2\right) \tag{3.13}$$

$$P_L = P_M + P_E \tag{3.14}$$

$$P_{out} = T_e \omega_r \tag{3.15}$$

$$\eta = \frac{P_{out}}{P_{out} + P_L} * 100 \tag{3.16}$$

In a conventional machine, operation under rated conditions is found to be highly efficient. This results from a favorable balance between copper and iron losses. However, there are many applications which require adjustable torque and speed different than the rated ones. A torque or speed far from the rated operating point causes a significant drop in the efficiency of IPMSM drive. This is due to the imbalance between iron and copper losses. Copper and

iron losses are the most fundamental and dominant losses in IPMSM [20]. Because of this, in model based efficiency optimization the value of R_c is calculated at the rated torque and speed. First the iron loss P_{Fe} is calculated by subtracting P_M, P_{cu} and P_{out} from the input power P_{in} and then equation (3.10) is solved for R_c. Usually the rated torque, speed, voltage, current and other necessary parameters are given in the motor name plates. Some manufacturers may not provide the rated torque and if that is the case the rated torque of the IPMSM can be calculated from (3.8). The complete parameter of the IPMSM which is under consideration for efficiency optimization in this thesis is given in Appendix A. As (3.15) depicted efficiency can be improved by minimizing P_L which is given by (3.13) where the mechanical loss P_M is not controllable, but the electrical loss P_E is controllable by means of current vector control. Based on (3.10-3.14) P_{Fe} can be calculated as follows:

$$P_{in} = P_{out} + P_L$$

$$= V_a * I_a * \cos\theta \tag{3.17}$$

$$P_{Fe} = P_{in} - P_M - P_{Cu} \tag{3.18}$$

Since, $P_{Fe} = R_c(i_d^2 + i_q^2)$ then Rc is derived as,

$$R_c = \frac{P_{Fe}}{(i_d^2 + i_q^2)} \tag{3.19}$$

Substituting (3.5) and (3.6) in (3.19) gives R_c as:

$$R_c = \frac{\omega^2(L_q^2 i_{oq}^2 + v_a^2 + 2L_d i_{od} v_a + L_d^2 i_{od}^2)}{P_{Fe}} \tag{3.20}$$

The variable i_{sq}, in the above equations can be eliminated by substituting (3.8) into (3.10) and (3.11) as shown in (40). Then, in the steady state operations where the speed and the torque are constant; the electrical loss becomes a function of i_{sd}, T_e and ω. The torque generating i_{sq} can be given as

$$i_{sq} = \frac{T_e}{P\left(\psi_a + \omega^2 L_d i_{sd}(1-\alpha)\right)} \tag{3.21}$$

Where, $\alpha = (1-\rho)$.

3.4 Basics of Efficiency Optimization Principle

In efficiency optimization control the motor's d-axis current and the air gap flux are reduced in order to achieve the lowest possible input power for the required torque and speed of IPMSM drive. The rotor air gap flux is decreased by reducing the magnetizing component of the stator current as a result of lowering the stator voltage in steps [21]. This ultimately results in a corresponding increase in the torque producing component of the stator current by the action of the speed controller so that the developed torque and speed remain constant at the desired values. As the air gap flux is decreased in steps, the iron core loss decreases as well. However, due to the rise in the torque component of the stator current, the copper

(resistive) loss increases [21, 22]. At the operating point where decrease in core loss is offset by the increase copper loss, the minimum input power level is reached. Any excursion past this point will cause the controller to return to the previous point. The basic idea is that, if the last control action indicates a decrease in input power, proceed decreasing in the same direction with the control magnitude somewhat proportional to the measured input power change. When efficiency the optimizer changes the motor's flux, there will be a corresponding change in the motor's rotor speed ω_r. Since the energy optimizer operates under the implied assumption of constant motor output torque and speed, any deviation from this premise is detrimental to the system's performance [20-23] as illustrated in Fig.3.2.

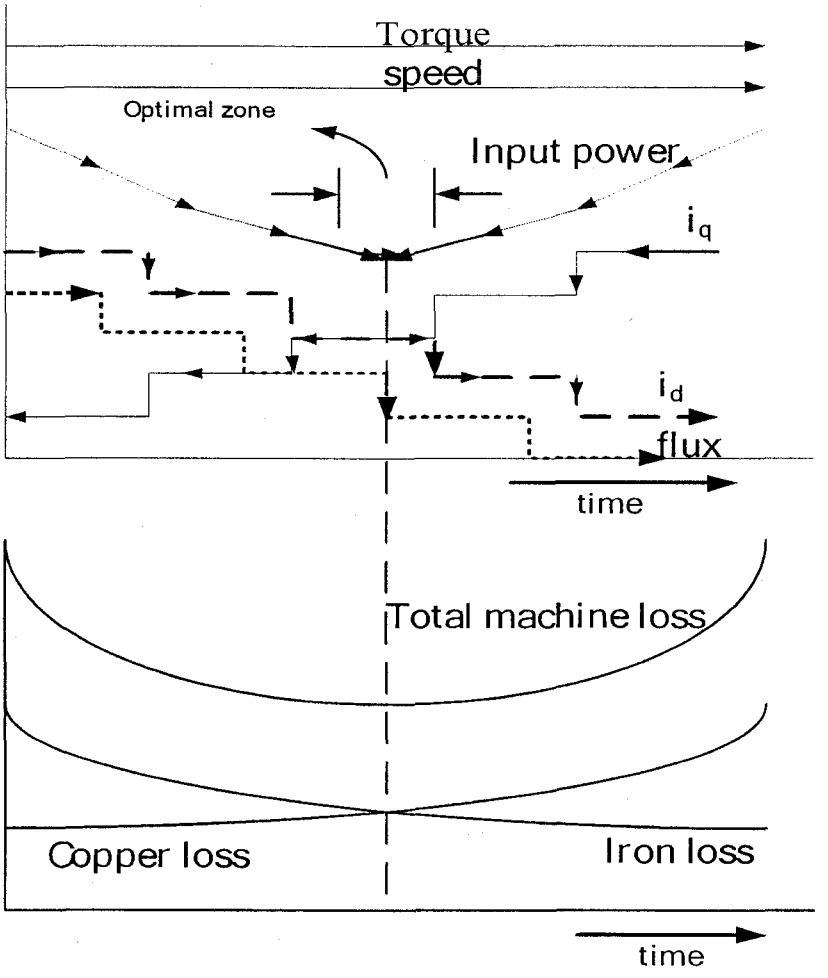

Fig. 3.2 An illustration of efficiency optimization control principle with d-axis current decrement.

3.5 The Proposed Efficiency Optimization Algorithm

The optimal operating point d-axis current which provides the minimum electrical loss can be found by partially differentiating P_E which is a function of i_{od}, T_e, and ω with respect to i_{od}.

$$\frac{\partial P_E}{\partial i_{od}} = 0, \text{ assuming } T_e, \omega = \text{Constant} \tag{3.22}$$

$$\frac{\partial^2 P_E}{\partial i_{od}^2} > 0, \text{ assuming } T_e, \omega = \text{Constant} \tag{3.23}$$

Equating the first derivative to zero insures that i_{od} gives either maximum or minimum motor loss at that operating point. Moreover, the second derivative of P_E with respect to i_{od} is always positive and this insures that i_{od} is the optimal d-axis current which provides minimum motor loss. Therefore, the efficiency optimization condition is that the first derivative of P_E with respect to i_{od} has to be equated to zero. These As a result, the loss minimization condition is given by,

$$X\,Y - T_e^2 Z = 0 \tag{3.24}$$

Where, X, Y and Z are given by (3.25-27) and T is given by equation (3.8), respectively.

$$X = P^2 \{R_a R_c^2 i_{od} + \omega^2 L_d (R_a + R_c)(L_d i_{od} + \psi_a)\} \tag{3.25}$$

$$Y = [\, \psi_a + (1 - \rho) L_d i_{od} \,]^3 \tag{3.26}$$

$$Z = \{ R_a R_c^2 + (R_a + R_c)(\omega \rho L_d)^2 \}(1 - \rho) L_d \tag{3.27}$$

For given torque T_e and speed ω the optimal d-axis current i_{od} is derived from (3.24) as shown below.

$$i_{od} = -A^{-1}\left(Bi_{od}^2 + Ci_{od}^3 + Di_{od}^4 - E\right) \tag{3.28}$$

Where, A, B, C, D and E are given as,

$$A = (\psi_a^3 \lambda + \omega^2 - 2i_{oq}^2 \rho^2 \psi_a L_d^4 \alpha\lambda\omega^2(R_s + R_c)$$

$$B=3((\omega^2 L_d^3(R_s + R_c)\psi_a^2\alpha)(1+\alpha) + L_d\psi_a^2\alpha\lambda) - 2i_{oq}^2 \rho^2\psi_a L_d^5\alpha^3\lambda\omega^2(R_s + R_c)$$

$$C = 3L_d^3\psi_a \alpha^2\lambda + 3\omega^2 L_d^4\alpha^2(R_s + R_c)\psi_a(1+\alpha)$$

$$D = L_d^3 \alpha^3\lambda + L_d^5\alpha^3\omega^2(R_s + R_c)$$

$$E = -i_{oq}^2 \rho^2\psi_a^2 L_d^3\lambda\omega^2\alpha$$

(3.29)

Substituting (3.29) in (3.28) gives us the General optimal d-axis for IPMSM as:

$$i_{od} = \frac{\left(3\left((\omega^2 L_d^3(R_s + R_c)\psi_a^2\alpha)(1+\alpha) + L_d\psi_a^2\alpha\lambda\right) - 2i_{oq}^2\rho^2\psi_a L_d^5\alpha^3\lambda\omega^2(R_s + R_c)\right)i_{od}^2}{(\psi_a^3\lambda + \omega^2 - 2i_{oq}^2\rho^2\psi_a L_d^3\alpha\lambda\omega^2(R_s + R_c)}$$

$$+\frac{\left(3L_d^3\psi_a\alpha^2\lambda + 3\omega^2 L_d^4\alpha^2(R_s + R_c)\psi_a(1+\alpha)\right)i_{od}^3}{(\psi_a^3\lambda + \omega^2 - 2i_{oq}^2\rho^2\psi_a L_d^3\alpha\lambda\omega^2(R_s + R_c)}$$

$$+\frac{\left(L_d^3\alpha^3\lambda + L_d^5\alpha^3\omega^2(R_s + R_c)\right)i_{od}^4}{(\psi_a^3\lambda + \omega^2 - 2i_{oq}^2\rho^2\psi_a L_d^3\alpha\lambda\omega^2(R_s + R_c)}$$

$$+\frac{-i_{oq}^2 \rho^2 \psi_a^2 L_d^2 \lambda \omega^2 \alpha}{(\psi_a^2 \lambda+\omega^2-2i_{oq}^2 \rho^2 \psi_a L_d^2 \alpha\lambda\omega^2(R_a+R_c)} \tag{3.30}$$

Where, $\lambda = R_a R_c^2$, $\alpha = (1-\rho)$

If the motor under consideration is nonsalient SMPMSM i.e. ($L_q = L_d$) then the Z term in (3.24) becomes 0, the Y term becomes ψ_a^2 and then the condition X=0 will give the simplified optimal d-axis current i_{od} as shown in (3.31). In this case the optimal current i_{od} is independent of the torque and easier to calculate.

$$i_{od} = -\frac{\omega^2 Ld(R_a+R_c)\psi a}{R_a R_c^2+\omega^2 L_d^2(R_a+R_c)} \tag{3.31}$$

In the same way by equating ψ_a=0 the optimal d-axis current for SynRM can also be found.

3.6 Complete IPMSM Drive with Efficiency Optimization Algorithm

The block diagram of the proposed loss model based efficiency optimization of IPMSM drive is shown in Fig.3 and the details of each block are given in Appendix B. In this proposed vector controlled IPMSM drive, the speed controller is implemented using a classical proportion and integral (PI) controller in order to take the advantages of its simplicity and faster response [21]. The speed error is produced by comparing the actual speed with the command speed. The actual speed is measured, utilizing an optical encoder

mounted on the rotor shaft of the IPMSM. The PI controller has speed error as its input and the command current, i_q^* as its output. The PI speed controller is given by (2.28) and (2.29) in chapter 2.

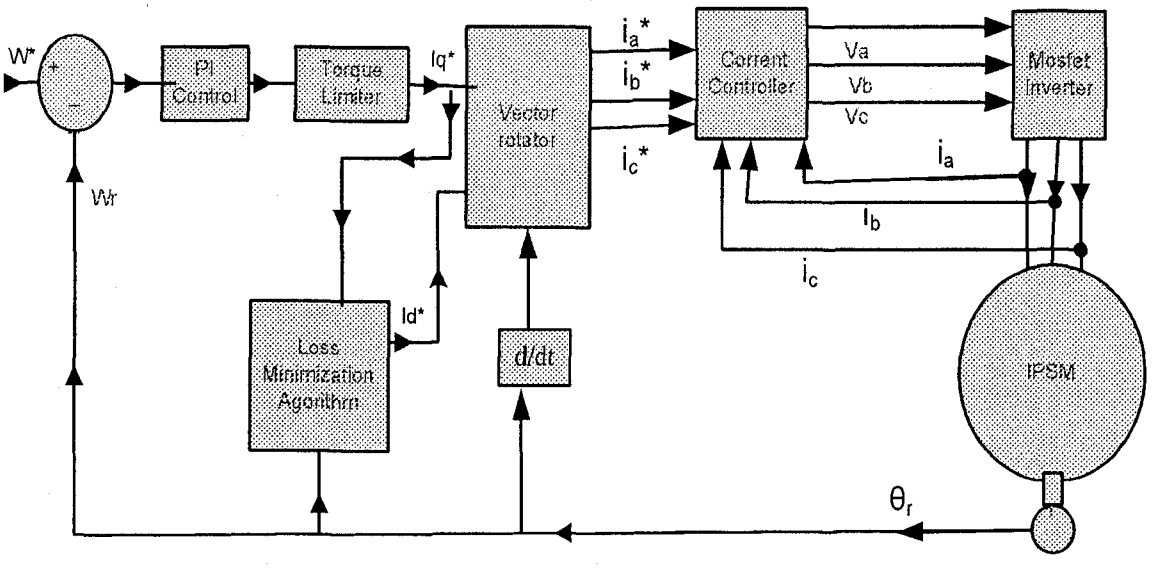

Fig.3.3 Block diagram of the proposed loss model based efficiency optimization of IPMSM drive.

The output of the loss minimization algorithm block is i_d^*. The command phase currents i_a^*, i_b^* and i_c^* are generated from i_q^* and i_d^* using the inverse parks transformation. The hysteresis controller compares the actual phase currents with corresponding command currents to generate PWM logic signals. These signals trigger the IGBT gates of the inverter in order to supply the IPMSM with appropriate voltage and frequency. The complete closed loop vector controlled IPMSM drive with the proposed loss minimization algorithm is simulated using Matlab/Simulink [32] according to Fig.3.3 and the Simulink block diagram is shown in Appendix B.3.

3.7 Simulation Results

The complete closed loop vector controlled IPMSM drive with the proposed loss minimization algorithm is simulated using Matlab/Simulink [32] according to Fig.3.3.The proposed loss minimization control algorithm is tested under different operating conditions such as sudden change in command speed, load and parameter variations, extra and some results are presented below. Figs. 3.4 and 3.5 show the simulated responses of IPMSM drive with proposed loss minimization and i_d=0 control, respectively in order to see the responses for a step increase in speed and load conditions. Initially, a step input of speed from zero to 100 rad/s with a load of 10 Nm is applied and then at t=0.5 s the load is increased from 10 Nm to 19 Nm. Again at t= 0.6 s, the command speed is increased from 100 rad/s to 180rad/s while a constant load of 19 Nm is applied. Fig.3(a) shows the speed response of the IPMSM drive with the proposed loss minimization controller and Fig.3(b) shows the speed response with the conventional i_d=0 control. It is seen from Fig.3(a) that the actual motor speed follows the command speed smoothly without any overshoot/undershoot and steady-state error for the proposed loss minimization algorithm. Whereas, for the conventional i_d=0 control the speed response suffers from overshoot/undershoot and exhibits slight steady-state error, which is not acceptable for high performance drive applications. The increase in load at t=0.5 s can be seen from the increase in torque and i_q from (Figs. 4(b) and 5(b)). The speed response for the proposed control is almost insensitive whereas, for the conventional i_d=0 control there is dip in the speed response when the load is increased. For the proposed control, d-axis current is adjusted with the changing load condition to optimize the efficiency, which can be seen from Figs.3(c) and 3(d). Whereas, for the conventional control as i_d=0 always remains zero, the efficiency drops with the step change in command speed which can

be seen from Figs.3.4(c) and 3.4(d). It is found from Figs.3.4(d) and 3.5(d), that an efficiency improvement of about 4% can be achieved with the proposed loss minimization algorithm as compared to the conventional i_d=0 control technique.

The change in parameter, particularly, the change in the value of L_q is a common phenomenon for IPMSM drives due to magnetic saturation. In order to see the responses of the proposed loss minimization algorithm with parameter variation; some simulation results are presented in (Figs.3.6 (a)-(d)). The value of L_q is decreased by 50% at t=0.5 s while the motor was running at rated speed of (183 rad/s) and rated load (19 Nm) conditions. It is clear from Fig. 3.6(a) the speed response is insensitive to the parameter change even if the value of L_q is decreased by 50% at t=0.5 s. Figs.3.6(b) and 3.6(c) show the corresponding variations in d and q axes currents, respectively. As shown in Fig.3.6(b) there is negligible variation in i_q for the applied parameter change which signifies the robustness of the proposed algorithm with less torque ripple and good speed response. It can be seen from Fig.3.6(c) that as L_q is decreased at t=0.5s the value of i_d is increased to compensate for the required torque demand by increasing the reluctance torque, while i_q is kept constant. This exhibits again the robustness of the drive. It is also found from Fig.3.6 (d) that the proposed controller can maintain the efficiency almost at its original level despite the variation in parameter. Figs.3.7 (a) and (b) show the total losses variations with proposed loss minimization algorithm and id=0 control, respectively, then as the parameter $L_{q\,is}$ decreased by 50% at t=0.5s while the motor was running at rated speed of 183 rad/s and at a rated load of 19Nm. Fig.3.7 depicted that the proposed loss minimization algorithm reduces the total motor loss significantly as compared to the conventional i_d=0 technique. Therefore the proposed loss minimization based controller is found to be robust while maintaining the efficiency at its optimal level against different operating conditions such as sudden load change, step change of speed, and

parameter variations. Fig.3.8 shows speed, efficiency, total loss and current responses for IPSM drive with the proposed loss minimization algorithm

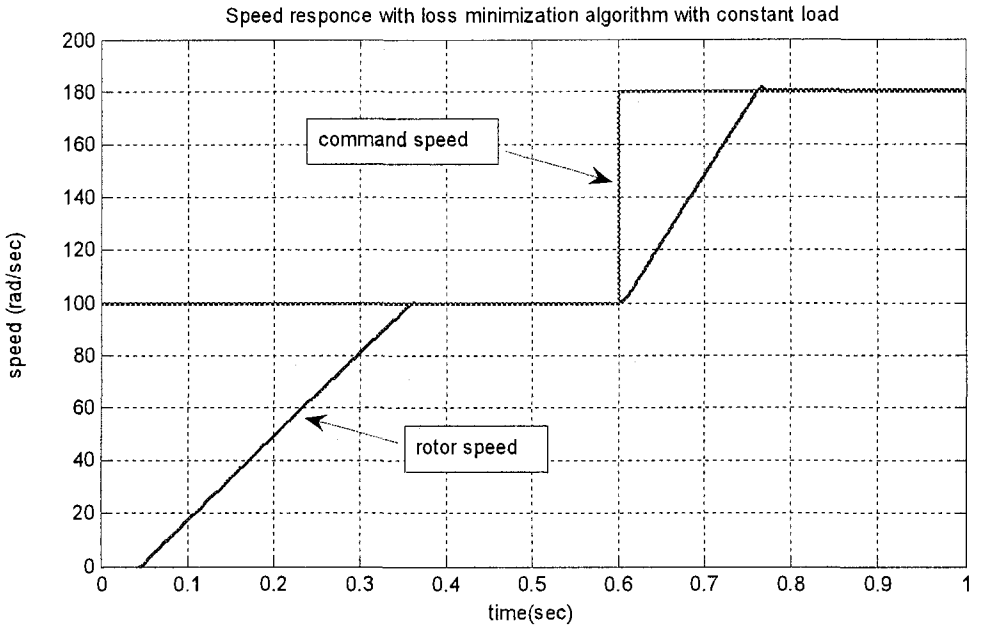
Speed responce with loss minimization algorithm with constant load
speed (rad/sec)
time(sec)
command speed
rotor speed
0
20
40
60
80
100
120
140
160
180
200
0.1
0.2
0.3
0.4
0.5
0.6
0.7
0.8
0.9
1

(a)

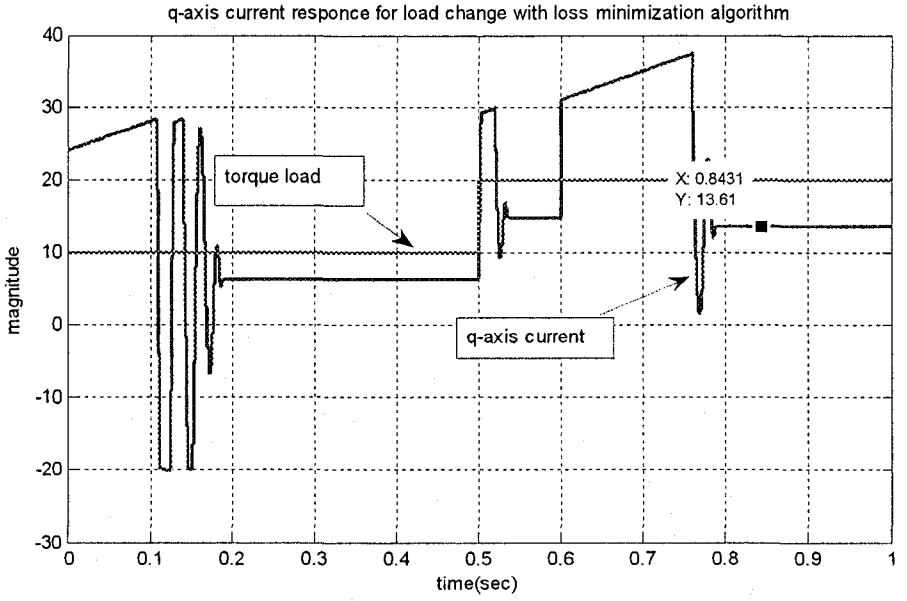
q-axis current responce for load change with loss minimization algorithm
magnitude
time(sec)
torque load
q-axis current
X: 0.8431
Y: 13.61
40
30
20
10
0
-10
-20
-30
0
0.1
0.2
0.3
0.4
0.5
0.6
0.7
0.8
0.9
1

(b)

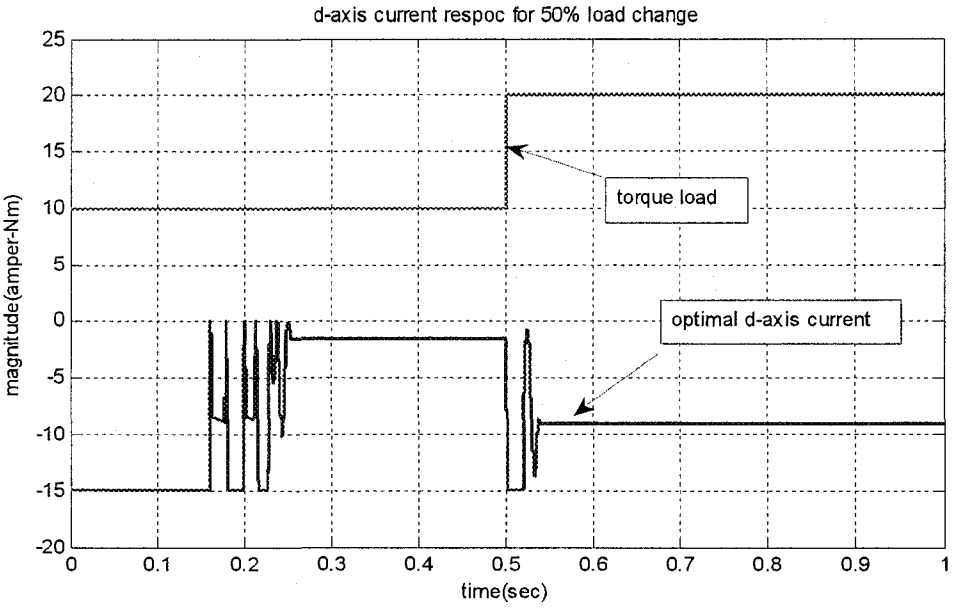

(c)

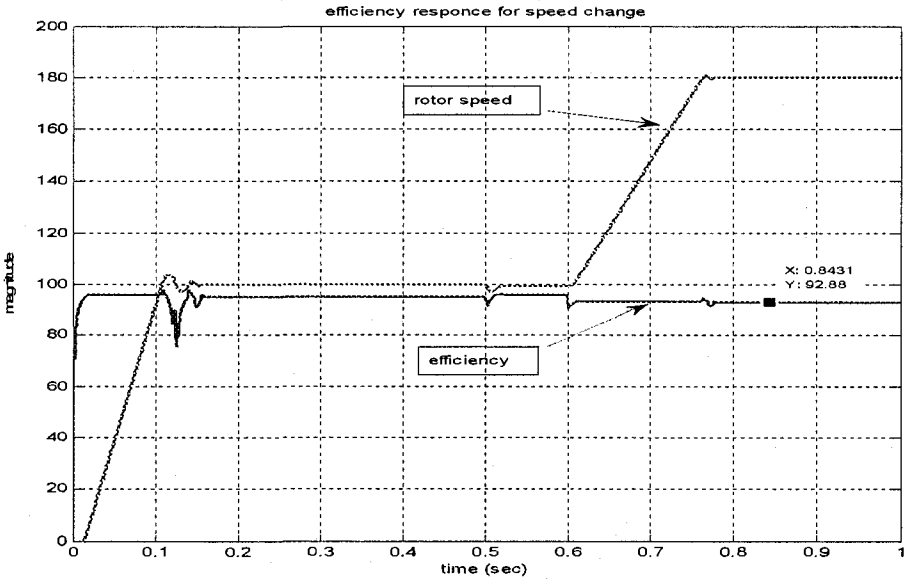

(d)

Fig. 3.4 Simulated responses of the proposed loss minimization based IPMSM drive; (a) speed, (b) i_q, (c) i_d and (d) efficiency.

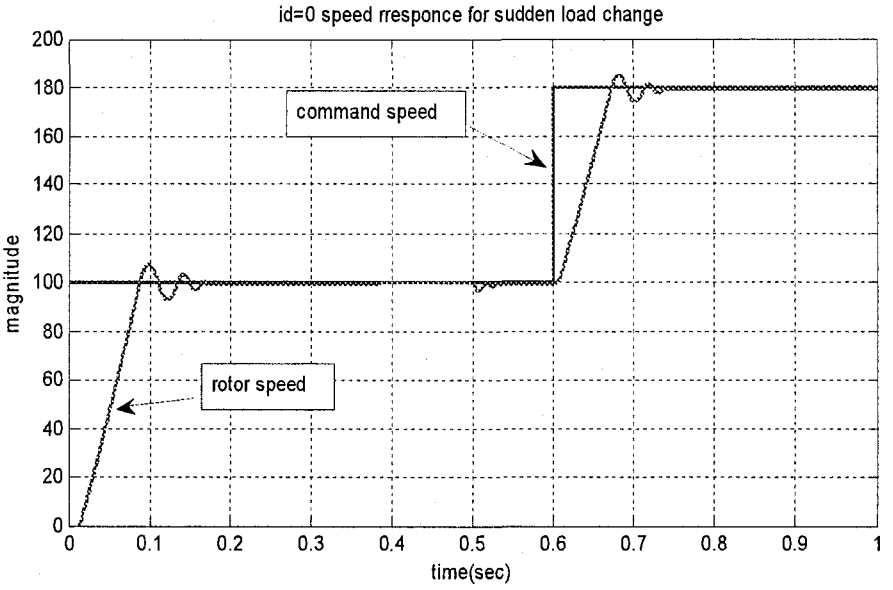
id=0 speed rresponce for sudden load change
command speed
rotor speed
magnitude
time(sec)
200
180
160
140
120
100
80
60
40
20
0
0
0.1
0.2
0.3
0.4
0.5
0.6
0.7
0.8
0.9
1

(a)

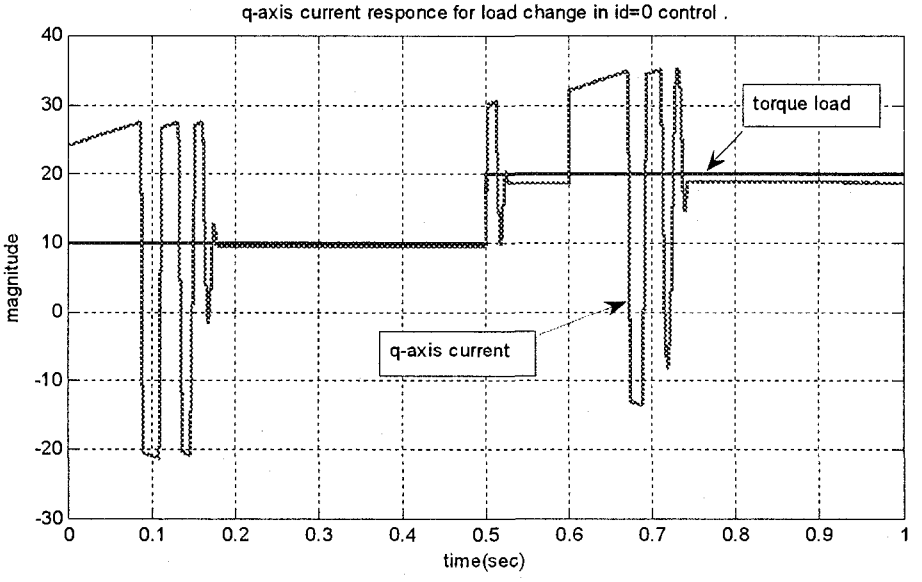
q-axis current responce for load change in id=0 control .
torque load
q-axis current
magnitude
time(sec)
40
30
20
10
0
-10
-20
-30
0
0.1
0.2
0.3
0.4
0.5
0.6
0.7
0.8
0.9
1

(b)

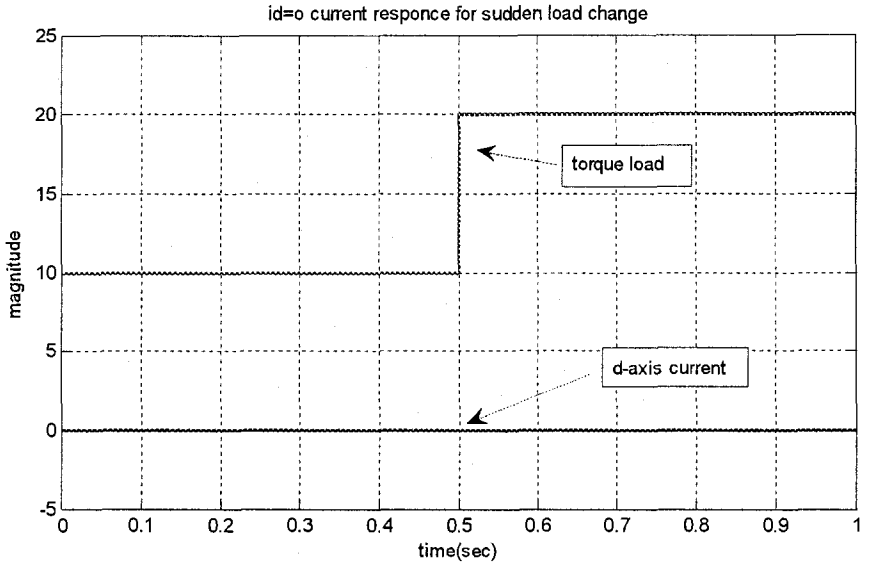

(c)

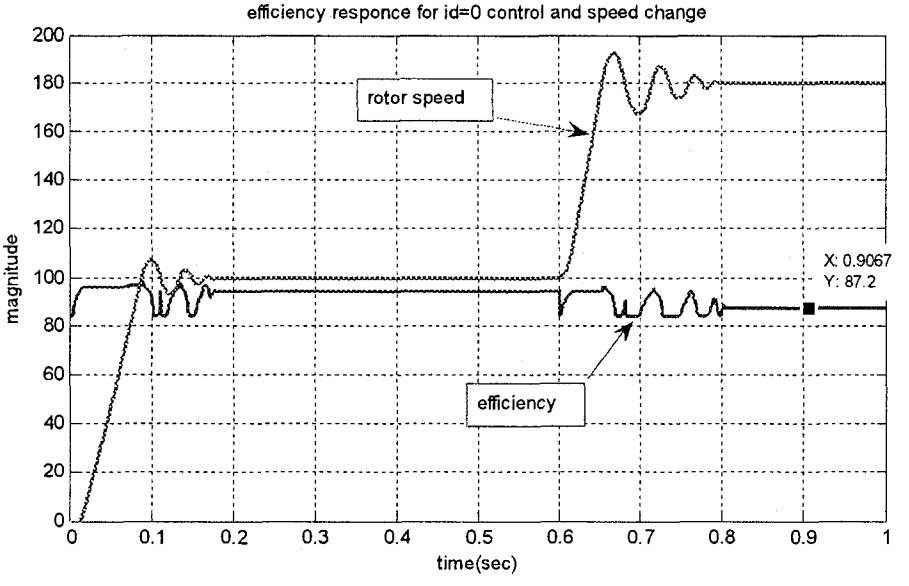

(d)

Fig. 3.5 Simulated responses of IPMSM drive with i_d=0 control technique; (a) speed, (b)i_q, (c) i_d and (d) efficiency.

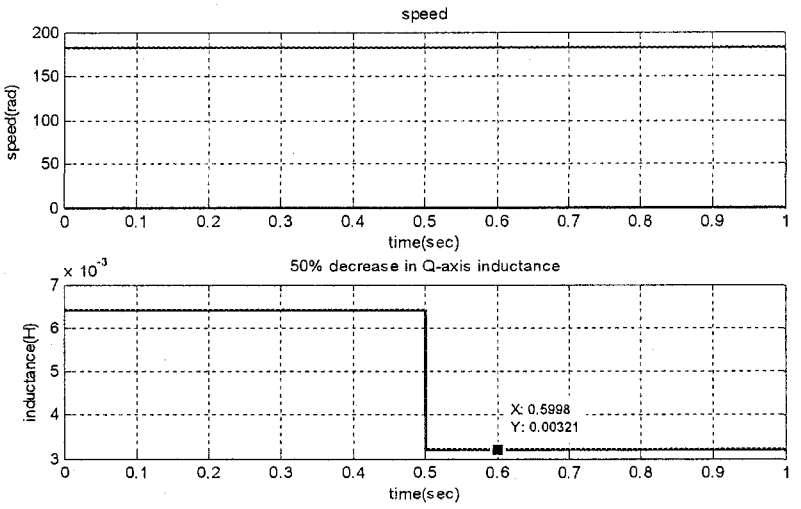
speed
speed(rad)
time(sec)
50% decrease in Q-axis inductance
x 10^-3
inductance(H)
X: 0.5998
Y: 0.00321
time(sec)

(a)

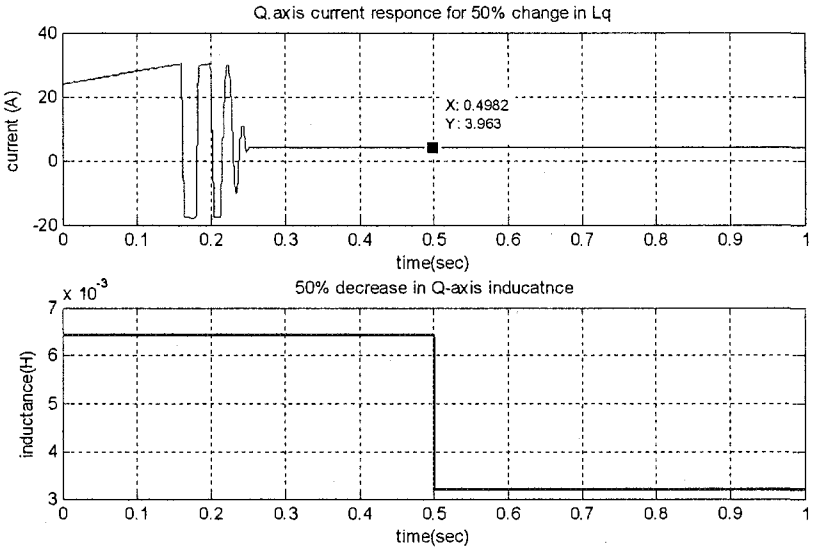
Q.axis current responce for 50% change in Lq
current (A)
X: 0.4982
Y: 3.963
time(sec)
50% decrease in Q-axis inducatnce
x 10^-3
inductance(H)
time(sec)

(b)

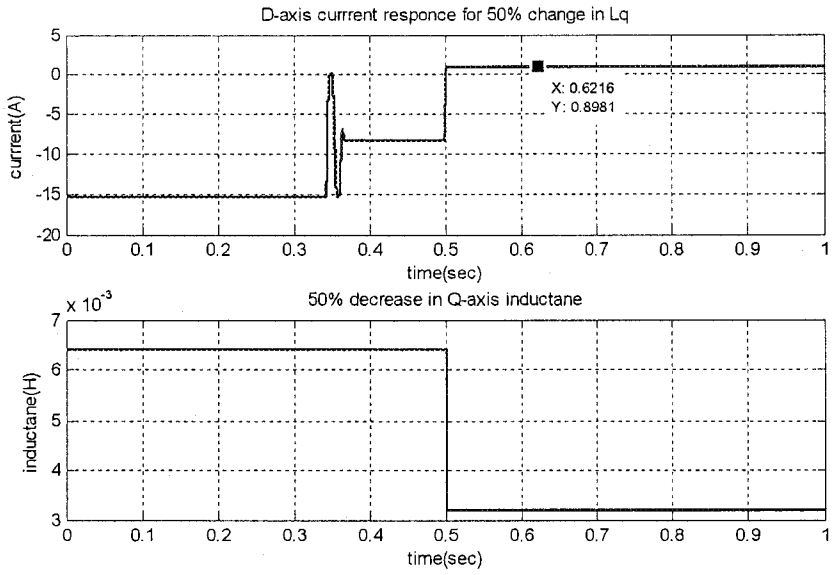

(c)

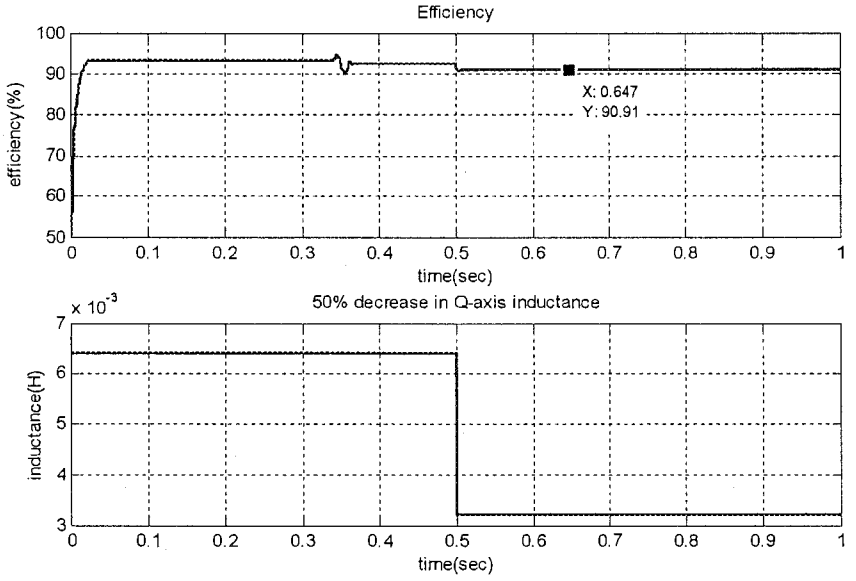

(d)

Fig.3.6 Simulated responses of IPMSM drive with parameter change for proposed loss minimization algorithm: (a) speed, (b)i_q, (c) i_d and (d) efficiency.

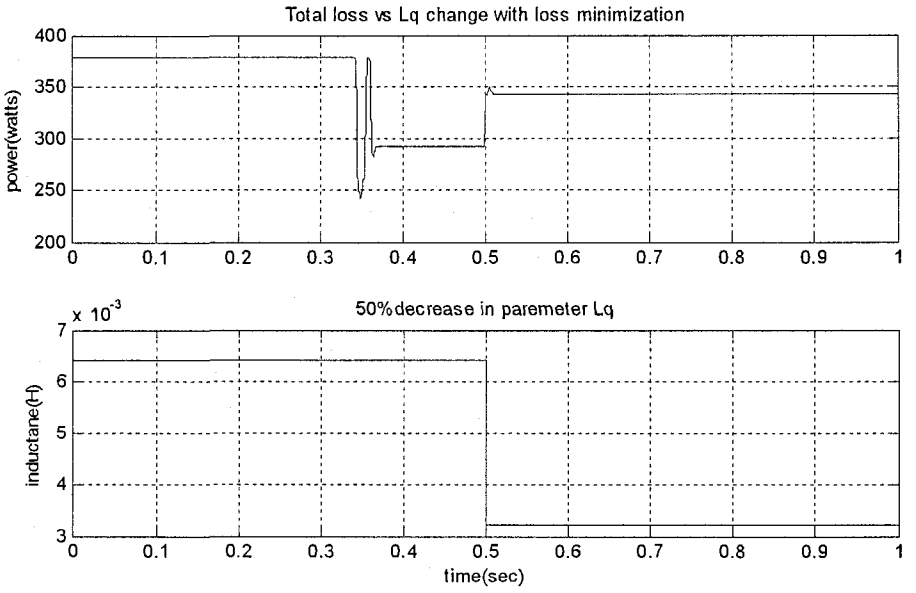

(a)

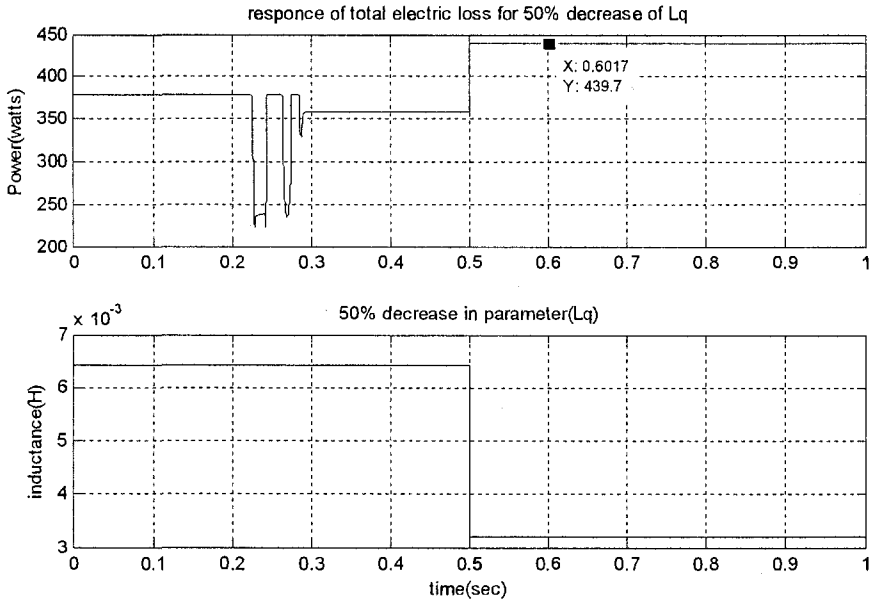

(b)

Fig.3.7 Simulated total loss for IPMSM drive while parameter L_q changes: (a) proposed loss minimization algorithm (b) i_d=0.

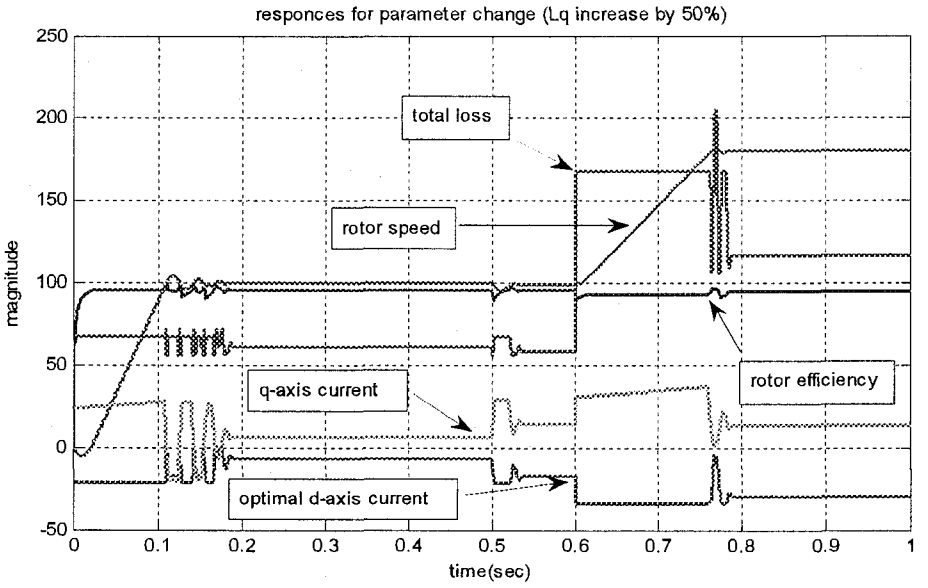

Fig.3.8 Simulated speed, efficiency, total loss and currents responses for IPSM drive with the proposed loss minimization algorithm.

Chapter 4

4.1 Experimental Implementation

After the performance of the IPMSM drive had been tested extensively in simulation, the results of the proposed drive were found to be satisfactory to be implemented in real time. The proposed loss minimization algorithm is implemented and the experimental results coincide with the simulation result as expected and some sample experimental results are presented. During the real time implementation the following assumption is taken into consideration in order to determine some motor parameters which were not available due to lack of accurate torque and voltage sensor and their driver circuitries compatible with the available DS1104 real time interface tool. All the experimental results are at steady state condition. First the motor is allowed to run at a certain command speed until it reaches steady state and then the stator phase voltage is measured. Once the stator phase voltage for that particular speed and load condition is found, it is feed back to the efficiency optimization algorithm as a real time feed back because the efficiency optimization algorithm requires a real time feedback of the developed torque and stator phase voltage in order to optimize the motor drive. Since a continuous real time T_e and V_a are not available at the moment of the experiment the transient responses of the IPMSM can't be captured and presented.

4.2 Experimental Set up

In order to implement the control scheme in real time the DSP board DS1104 is used [33]. The DS1104 board is mainly based on a Texas Instrument MPC8240 64-bit floating point digital signal processor. The DSP is supplemented by a set of on-board peripherals used in digital control systems including analog to digital (A/D), digital to analog (D/A) converters and incremental encoder interfaces. Also, it is equipped with a TI TMS320F240 16-bit micro controller DSP that acts as a slave processor and provides the necessary digital I/O ports and powerful timer functions such as input capture, output capture and PWM signal generation.

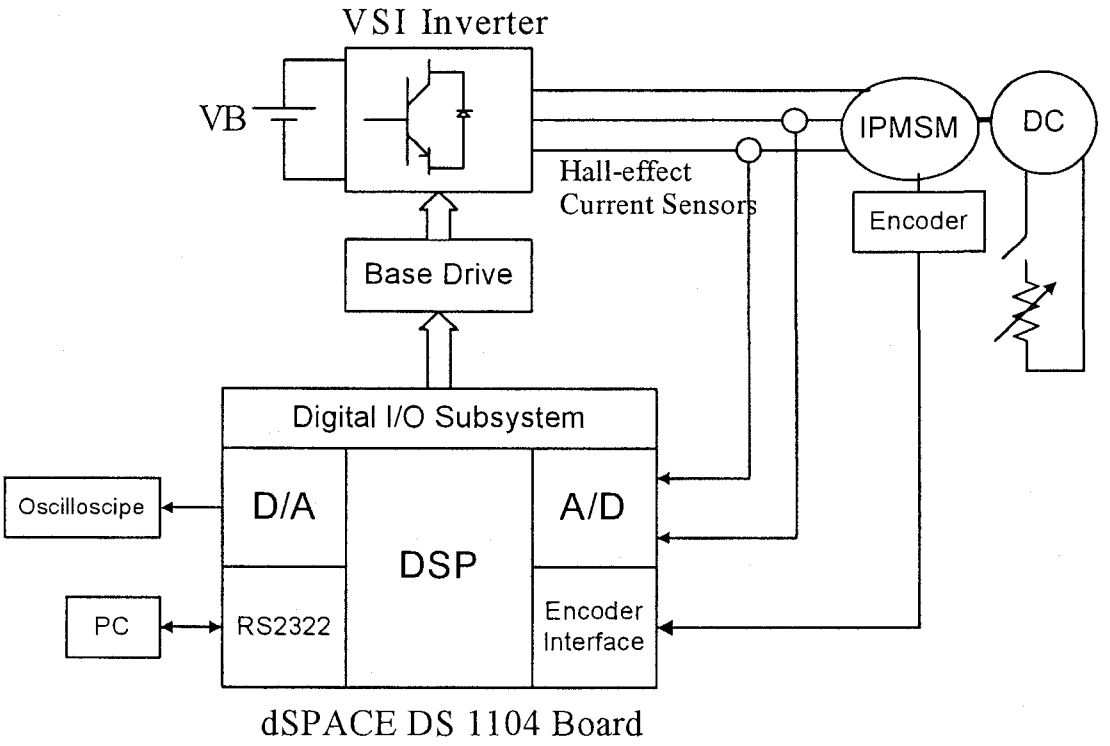

Fig. 4.1 Block diagram of the hardware schematic of the VSI-fed IPMSM drive.

The block diagram of the hardware schematic is shown in Fig. 4.1. The actual motor currents are measured by the two Hall-effect sensors and then fed back to the DSP board through the

A/D channel. Once the two phase currents are received through the A/D channel and scaled to their real time value the third phase current will be calculated in software. Rotor position is sensed by an optical incremental encoder mounted at the rotor shaft and is fed back to the DSP board through the encoder interface. The outputs of the DSP board are six PWM signals that are sent directly to the base drive circuit of the inverter. In order to implement the efficiency optimization algorithm, a real-time Simulink model for the complete drive system is developed. Then the model is downloaded to the DSP board using the Control Desk software. After initializing all the required variables, the speed is calculated from the present and past samples of the rotor position angle. Then using the values of the measured currents, speed, speed errors, and the output from efficiency optimization algorithm and some motor parameters, the command currents are generated from the current controller block and feed to hysteresis band to generate the PWM signals. The block diagrams for real time implementation of the complete drive are shown in Appendix B.4 and 5.

4.3 Experimental Results

As shown in chapter 3 the proposed loss minimization control algorithm for IPMSM drive tested in simulation under different operating conditions such as sudden change in command speed, load and parameter respectively in order to evaluate its performance. Whereas, in this chapter the complete drive has been tested in real time experiment based on DS1104 digital signal processing board and sample results are presented below.

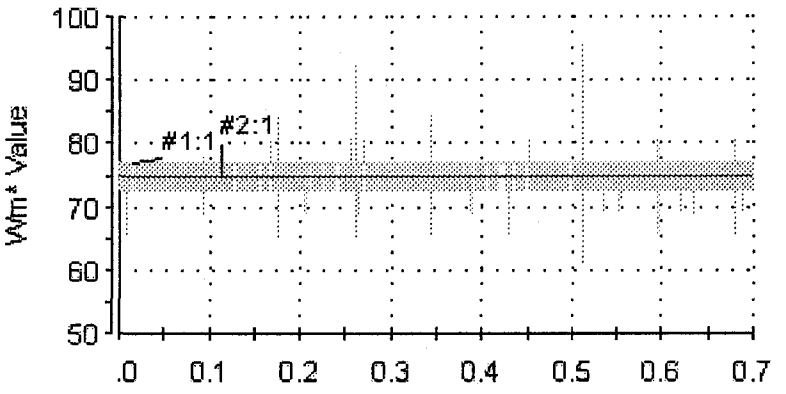
100
90
80
70
60
50
Wm* Value
#1:1
#2:1
.0
0.1
0.2
0.3
0.4
0.5
0.6
0.7

(a)

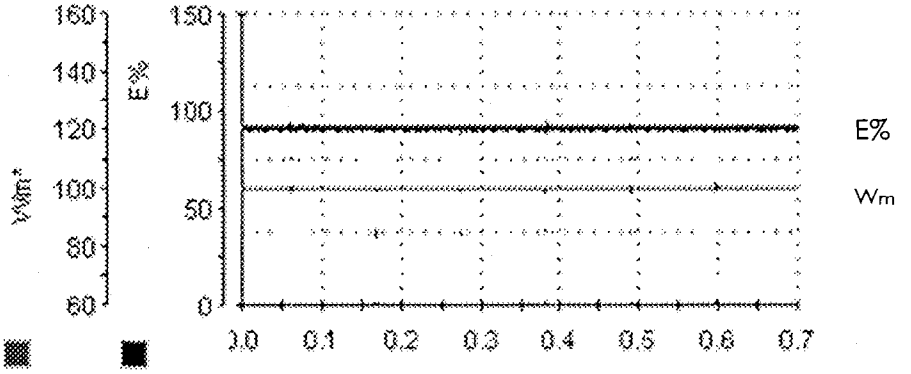
160
140
120
100
80
60
Wm*
E%
150
100
50
0
E%
Wm
0.0
0.1
0.2
0.3
0.4
0.5
0.6
0.7

(b)

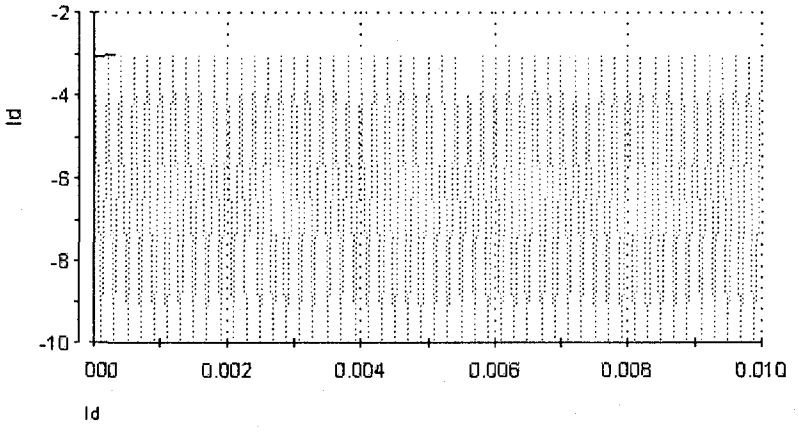
-2
-4
-6
-8
-10
Id
000
0.002
0.004
0.006
0.008
0.010
Id

(c)

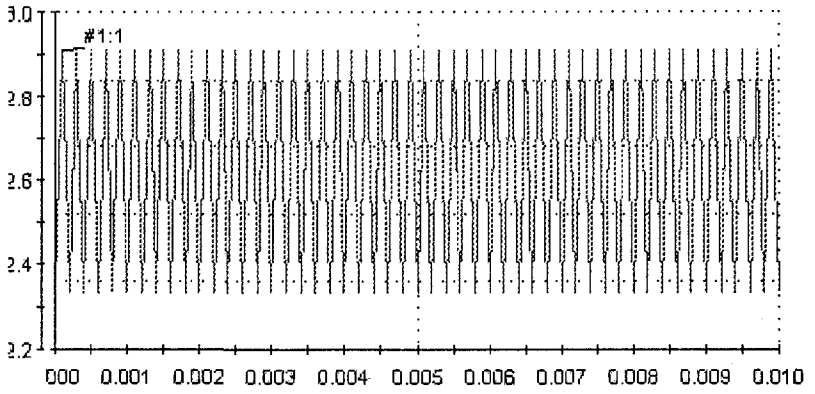

(d)

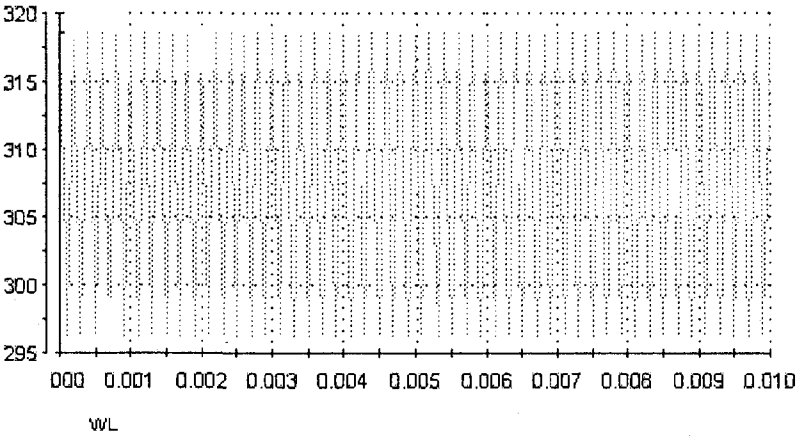

(e)

Fig.4.3 Real time responses IPMSM drive with efficiency optimization algorithm (a) speed, (b) efficiency, (c) i_d , (d) i_q and (e) P_L.

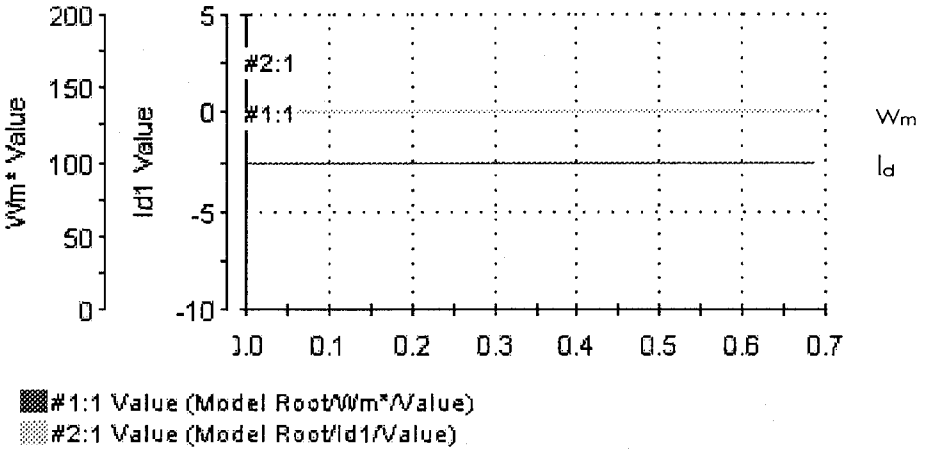

(a)

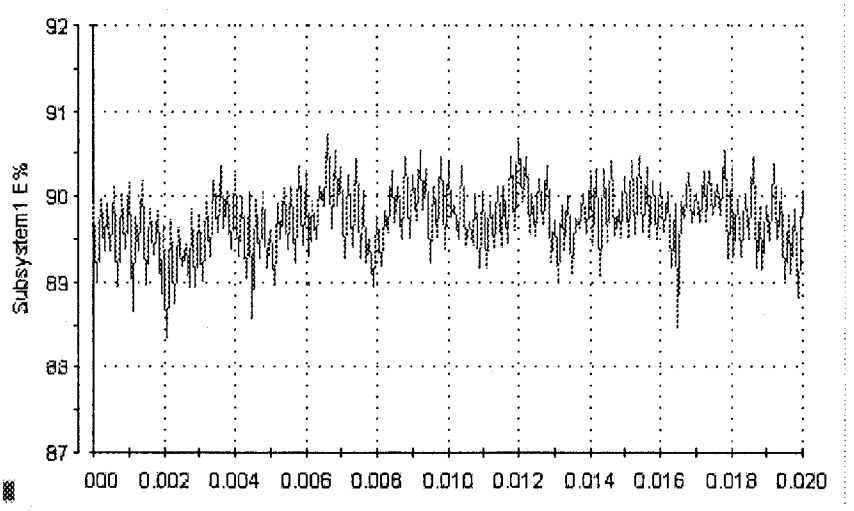

(b)

Fig.4.4 Real time responses IPMSM drive with id=0 control technique. (a) speed and (b) efficiency.

Figures 4.3 and 4.4 show the real time experimental responses of IPMSM drive with proposed loss minimization and with id=0 control technique, respectively. For the purpose of analyzing the responses for a given speed command and load conditions a step input of 75

rad/s speed command and a load of 19 Nm are applied as shown in Fig.4.3 (a) and the speed command is increased to 100 rad/s while the same constant load of 19 Nm is maintained as shown in Fig.4.3 (b). It can be seen from Fig.4.3 (a) that the actual motor speed follows the command speed smoothly without any steady-state error for the proposed loss minimization algorithm. Fig. 4.3(b) shows 93% efficiency for a speed command of 100rad/s as expected based on the previous simulation result. Figs.4.3(c)-(e) show the optimized i_d, i_q and P_L respectively, and they are in agreement with the simulation results found from the previous chapter. Fig.4.4 (a) shows a 100rad/s rotor speed and the un-optimized i_d current which is always zero because of the i_d=0 control technique and Fig.4.4 (b) shows the efficiency which is less than 90% at average and the efficiency has with lots of fluctuations in the real time response than the simulation one. Due to the time limitation the complete experimental testing was not done. However the available experimental results still verify the simulation that the proposed los minimization can improve the efficiency as compared to the conventional id=0 control technique.

Chapter 5

Conclusion

5.1 Conclusion

In this thesis a model based efficiency optimization control algorithm for vector-controlled IPMSM drive has been developed, simulated and implemented in real time. The developed efficiency optimization control algorithm determines the optimal d-axis current of the drive for a given speed and torque command, it is as fast as the vector-control and it has no torque ripple. All the real time responses are in conformity with the simulation results and the IPMSM drive efficiency is satisfactorily optimized in real time too. This efficiency optimization algorithm can also be used for surface mounted PM motor ($L_d = L_q$) and for synchronous reluctance motor ($\psi_{af} = 0$). The performance of the proposed optimization algorithm has been tested extensively both in simulation and real time experiment at different operating conditions such as sudden load change, command speed change and parameter change, etc. The proposed algorithm has also been compared with the conventional $i_d=0$ control scheme. The proposed efficiency optimization control algorithm showed significant improvement in efficiency as compared to the conventional $i_d=0$ control scheme. Thus, the proposed loss minimization algorithm has been found to be robust and efficient for high performance motor drive applications.

5.2 Future Scope

More research studies are being reported using the speed sensorless approach. Implementing speed sensorless will eliminate the need for an encoder as well as any difficulties associated with it. In addition to that it will be a good practice to apply the fuzzy logic controller instead of the conventional PI controller in order to exploit the outstanding advantage of fuzzy logic controller's ability of handling nonlinearity. Another technique which should be employed is the field weakening technique for wide speed range operation. In this work the efficiency optimizer is compared against the conventional $i_d = 0$ technique, which allows the motor to be controlled up to the rated speed. For control beyond rated speed, the field weakening technique must be used to calculate the command d-axis current and the performance of the proposed efficiency optimizer needs to be investigated for further robustness. Another point that worth mentioning is that as it is explained in many literatures the search efficiency optimization technique is more advantageous than the model based technique in handling the inherent parameter variation of IPMSM but can't be implemented alone because of its disadvantages like excessive torque ripple and very sluggish response therefore combining both the search optimization technique for steady state operation and the model based technique for the transition part could be an interesting research area for the future.

Appendix A

Appendix A.1 IPMSM Parameters

Number of poles	6
R_a	0.242ohm
L_q	6.42mH
ψ_a	0.24Wb
L_d	5.06mH
R_c	7.5ohm
f_{rated}	87.5Hz
I_a	14.2A
V_a	183
T_e	19.1Nm
T_{mech}	0.001
P_{rated}	5hp

Appendix B

Simulink block diagrams and details of different efficiency optimization algorithm subsystems.

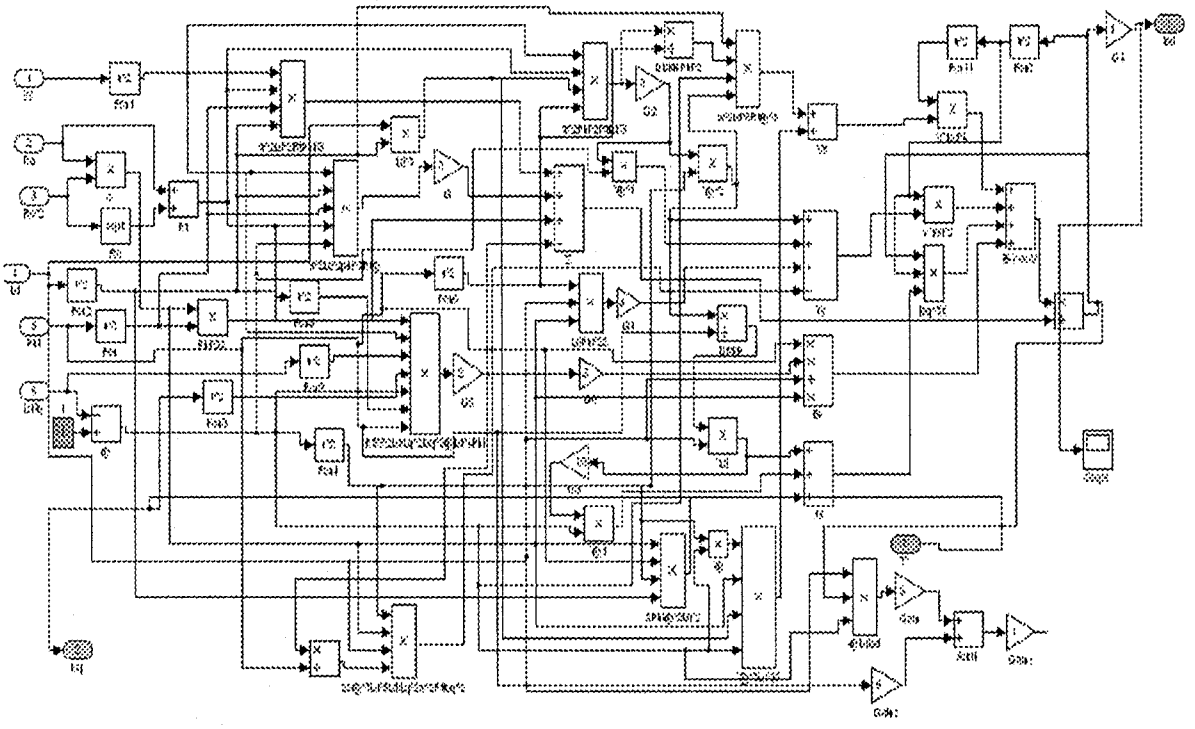

Appendix B.1 The loss minimization Simulink model.

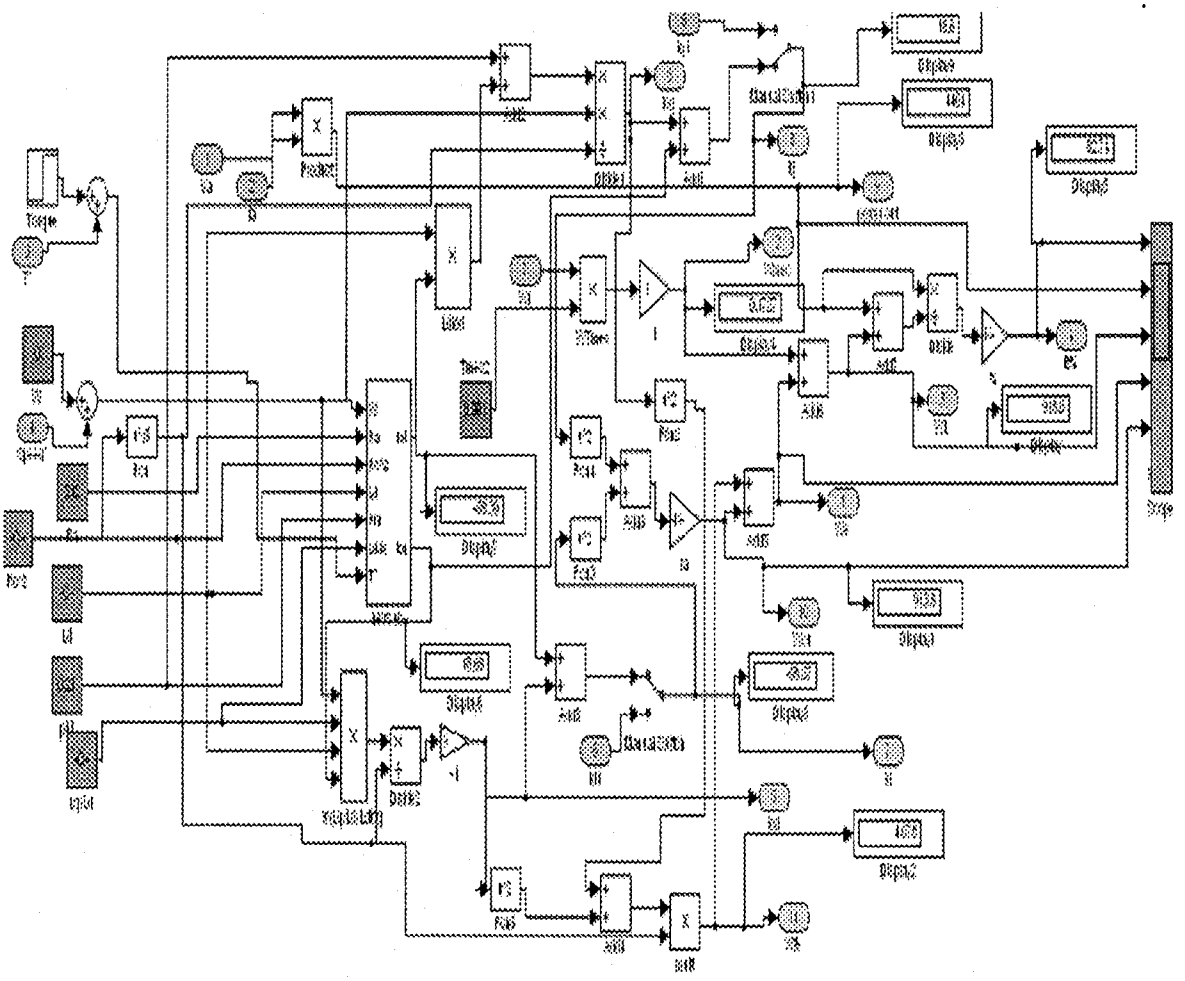

Appendix B.2 Loss minimization Simulink model.

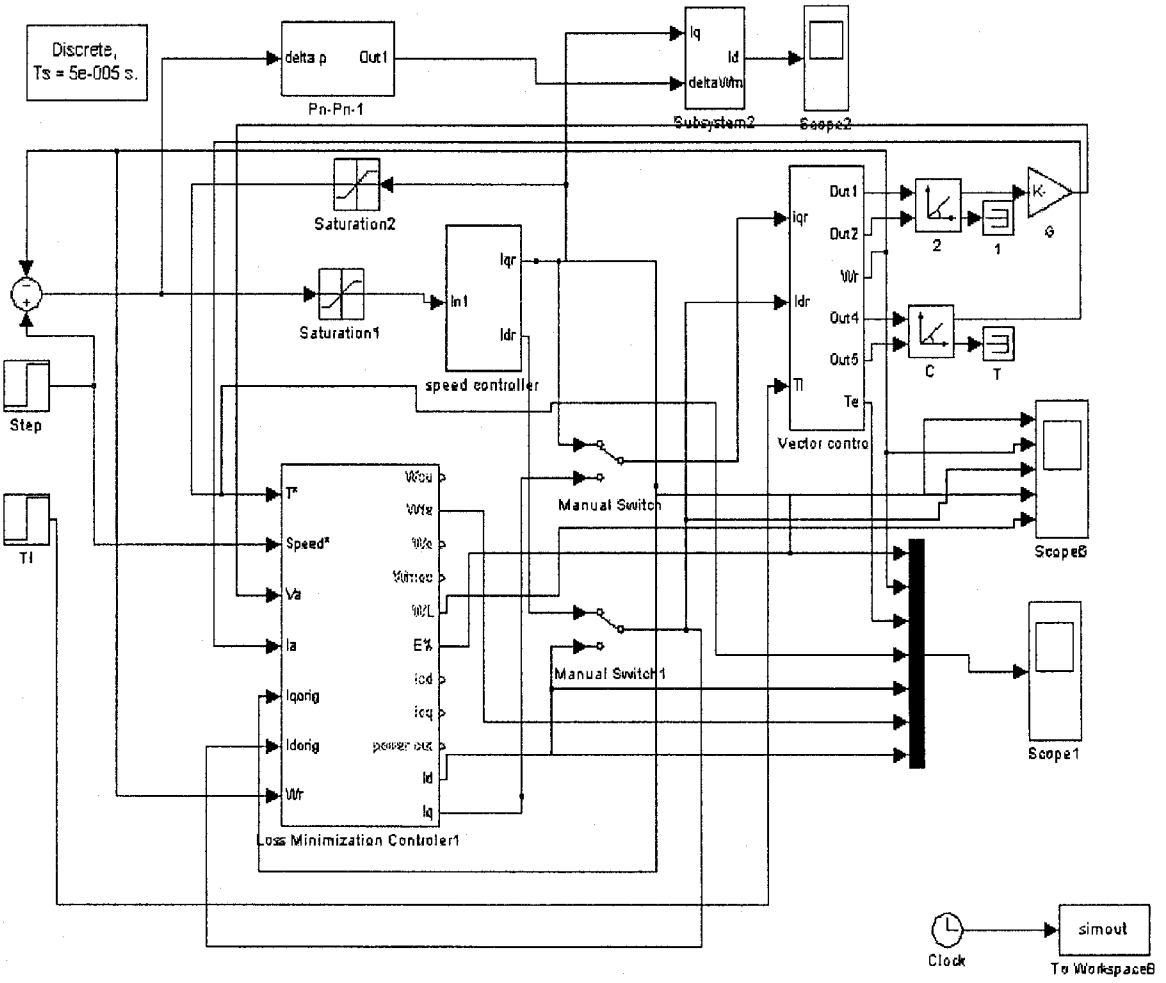

Appendix B.3 Complete Loss Minimization Model with Field oriented PM control.

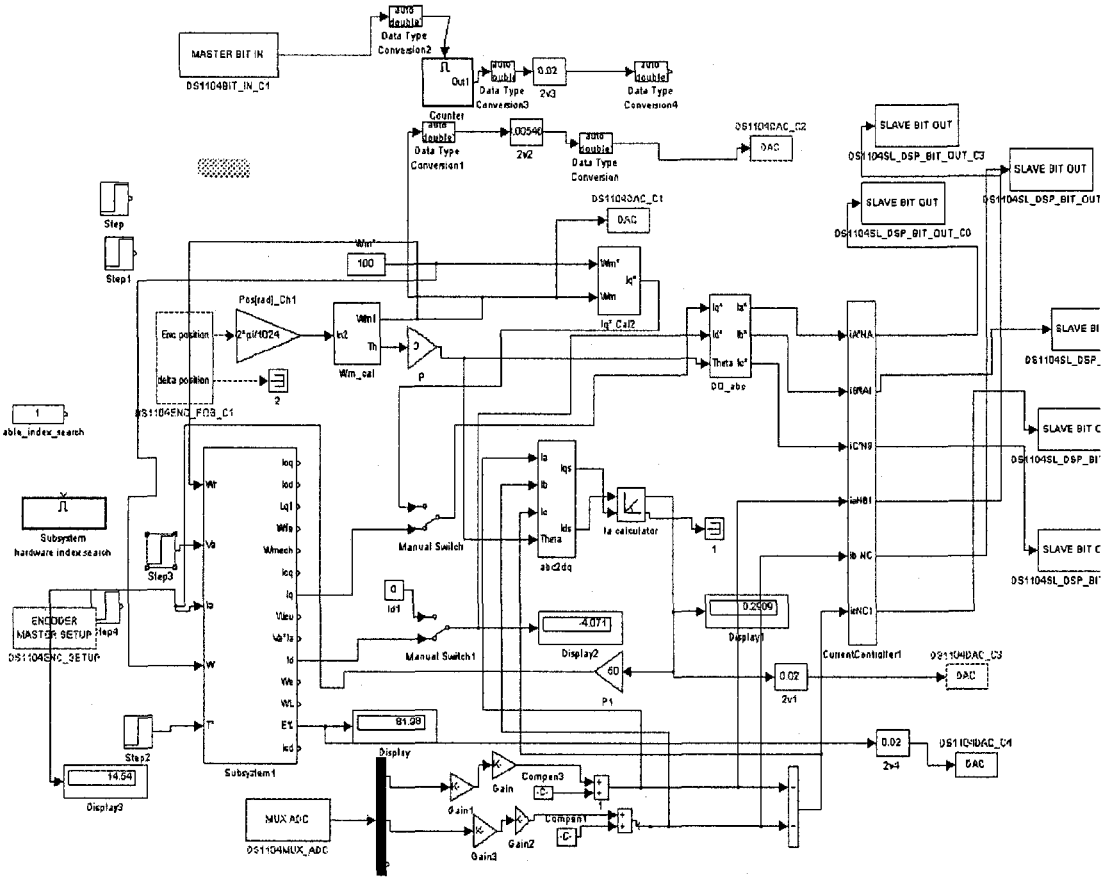

Appendix B.4 Real time Simulink and dspace block of the proposed efficiency optimization algorithm.

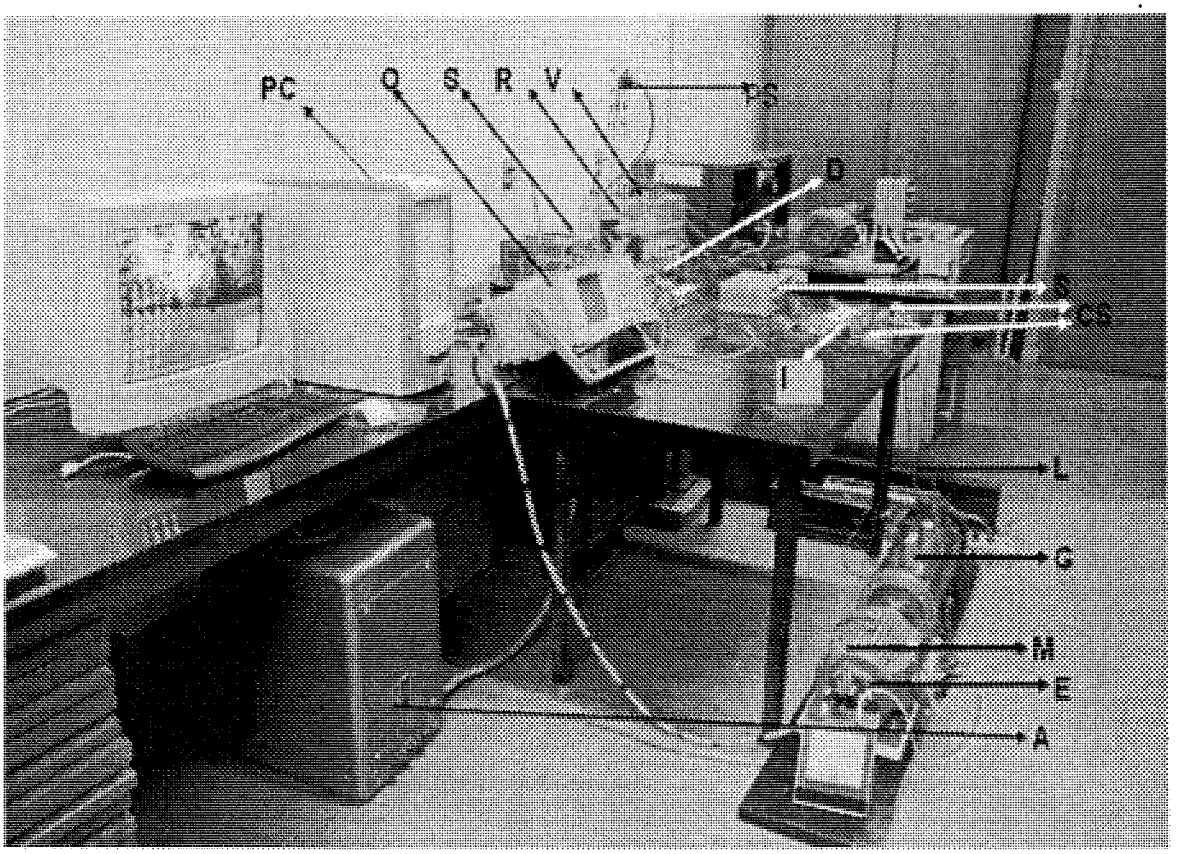

Appendix B.5 Experimental setup of the proposed efficiency optimizer of IPMSM drive

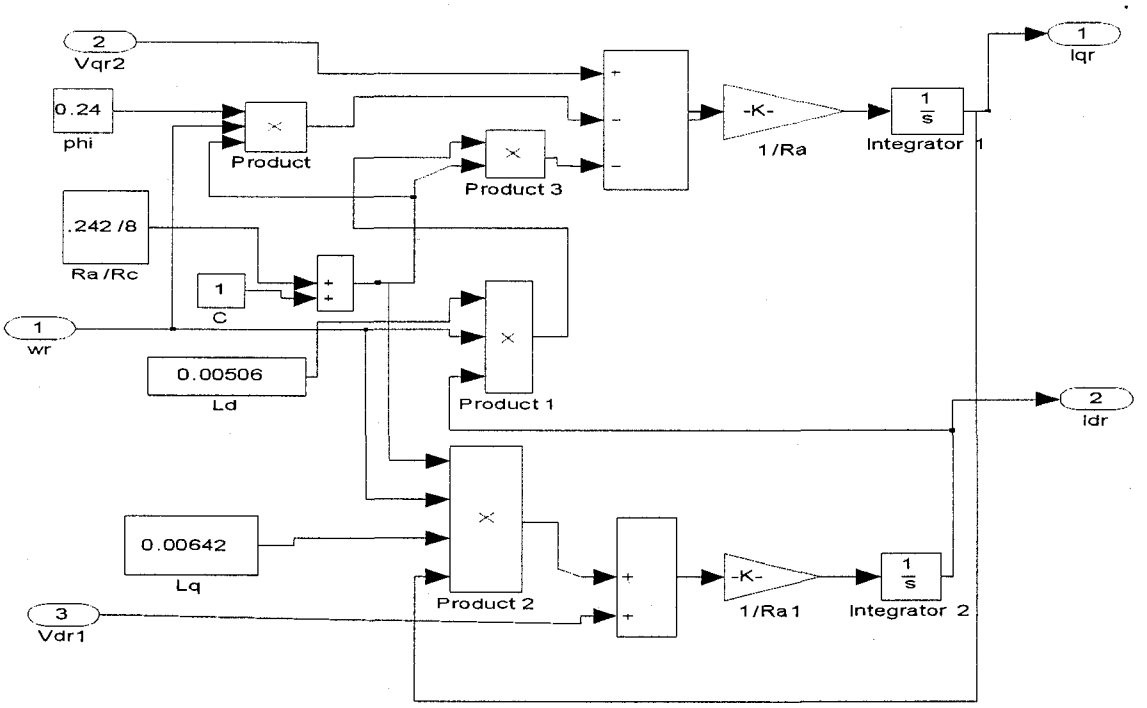

The Appendix B.6 d and q axis current calculator

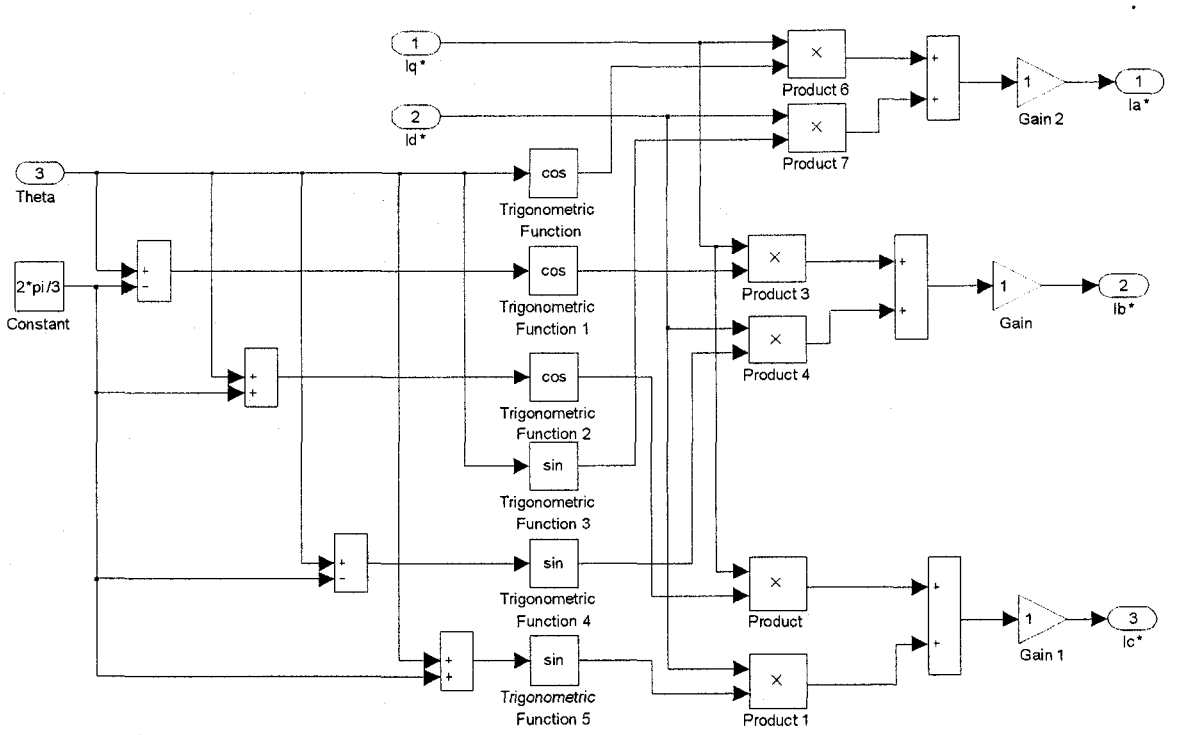

Appendix B.7 DQ—abc transformer.

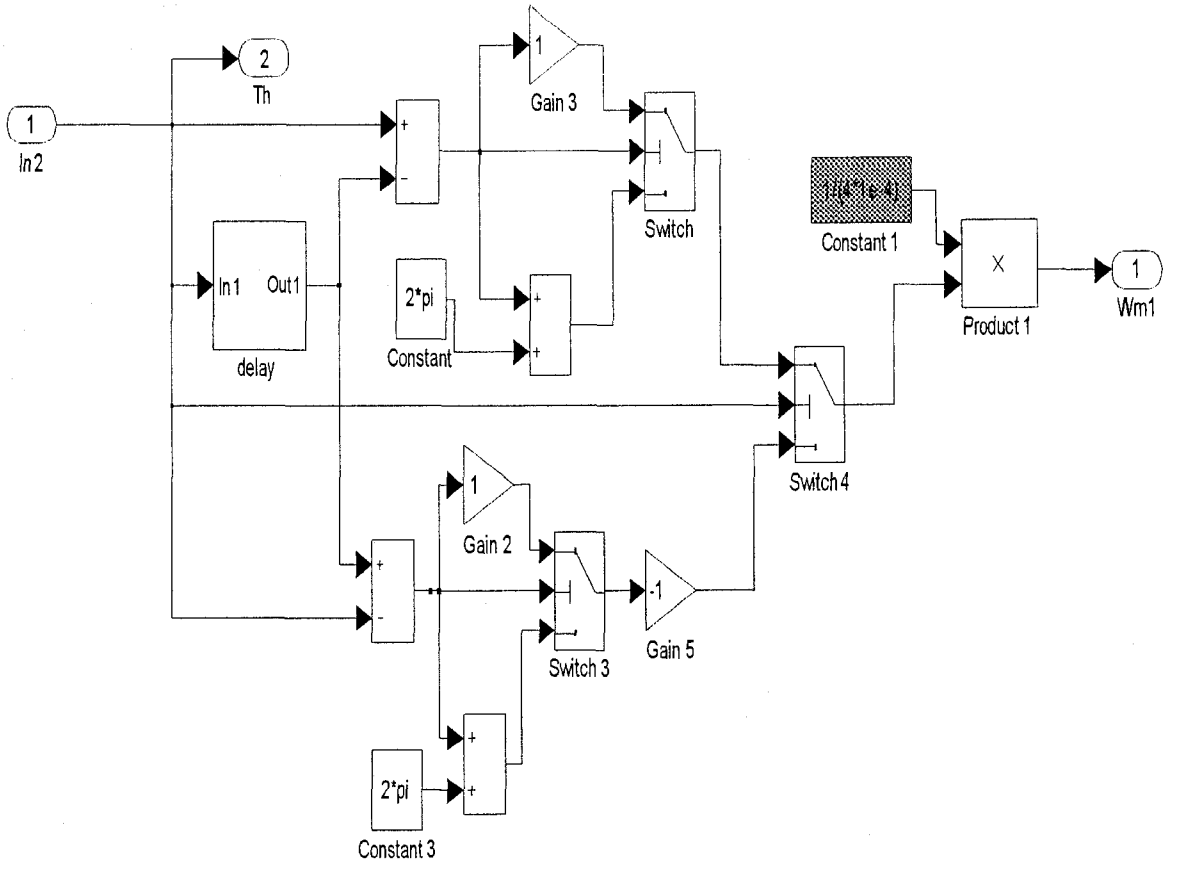

Appendix B.8 Speed calculator from the encoder position input.

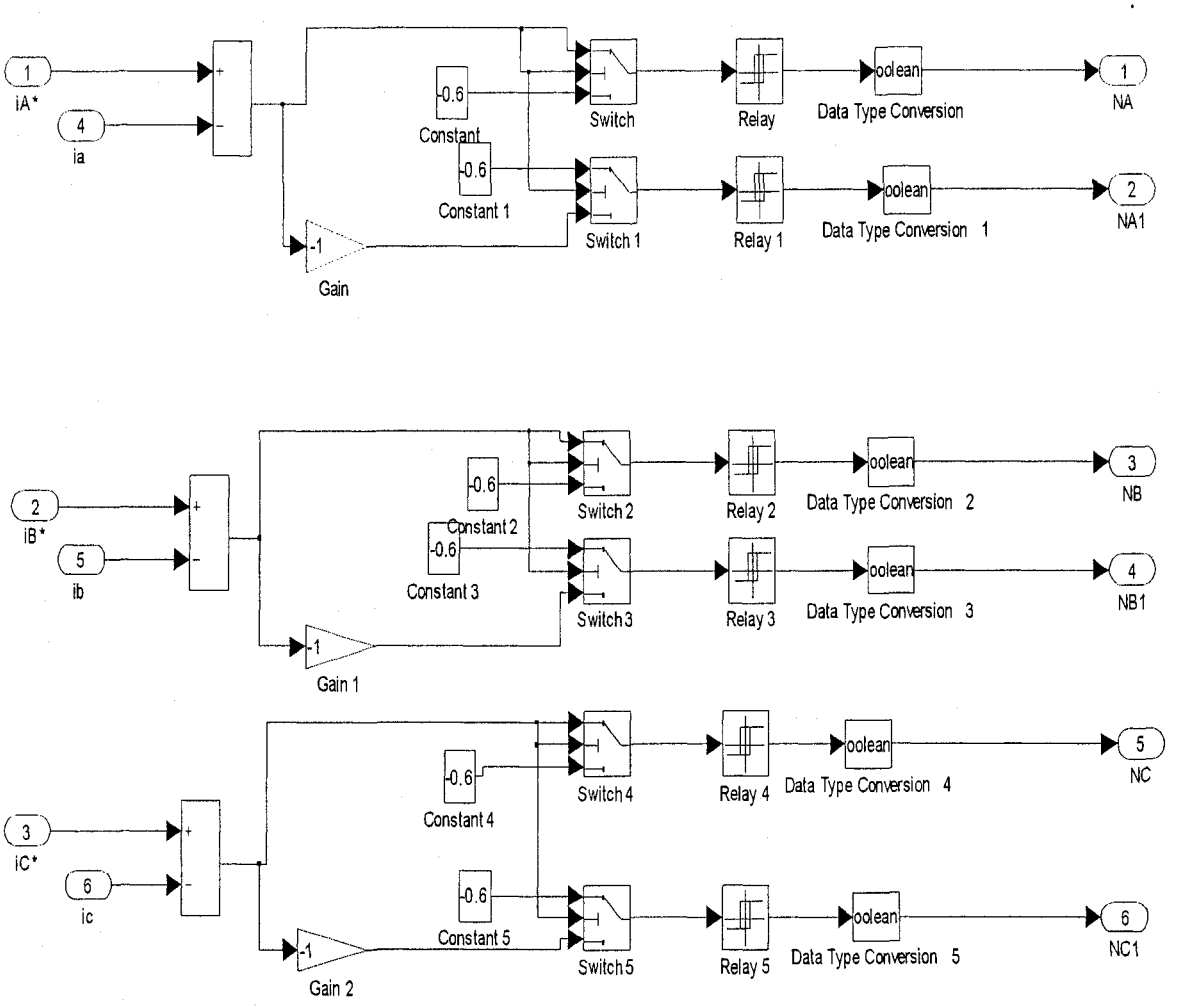

Appendix B.9 Real time Current controller and PWM signal generator.

References

[1] "Opportunities for Energy Savings in the Residential and Commercial Sectors with High- Efficiency Electric Motors," *Final Rep.*, Arthur D. Little, Inc., pp 1-15, United Kingdom Environmental Protection Agency,1999.

[2] S. Morimoto, Y. Takeda, T. Hirasa, and K. Taniguchi, "Expansion of operating limits for permanent magnet motor by current vector control considering inverter capacity," *IEEE Trans. Ind. Applicat.*, vol. 26, pp. 866–871, Sept./Oct. 1990.

[3] H.Murakami, Y.Honda, T.Higaki, S.Morimoto,Y.Takeda, "Rotor Design and Control method of Synchronous Reluctance Motor with Multi-flux Barrier",*Proceedings of Power Electronics Drives and Energy Systems for Industrial Growth,* pp.391-396,1998

[4] Andrzej M.Trzynadlowski, *The Field Orientation Principle in Control of Induction Motors*, Kluwer Academic, 1994.

[5] A. Abbondanti, "Methods of flux control in induction motors driven by variable frequency, variable voltage supplies," *in Conf Rec. Int. Semiconductor Power Converter Conf* 1977.

[6] T. M. Jahns, G. B. Kliman, and T. W. Neumann, "Interior permanent magnet synchronous motors for adjustable-speed drives," *IEEE Trans. Ind. Applicat.*, vol. IA-22, pp. 738–747, July/Aug. 1986.

[7] Y.HondaY H.Murakami, K.Narazaki, T.Higaki,S.Morimoto, Y.Takeda, "Optimum Design of a Multi Layer Interior Permanent Magnet Synchronous Motor Using Reluctance Torque", *Electrical Engineering in Japan,* vol.127, No.1, pp.249-259, April **15,**1999.

[8] M. A. Rahman and P. Zhou, "Analysis of brushless permanent magnet synchronous motors," *IEEE Transactions on Industrial Electronics*,vol. 43, no. 2, pp. 256-267, Apr. 1996.

[9] M. N. Uddin. And M. A. Rahman, "Fuzzy Logic Based Speed Control of an IPM Synchronous Motor Drive", Journal of Advanced Computational Intelligence, vol. 4 No. 3, pp.212-219.2000.

[10] M. N. Uddin, "Intelligent control of an interior permanent magnet synchronous motor," Ph.D. dissertation, Memorial University of Newfoundland, St. John, Oct. 2000.

[11] S. A.Nasar, I.Boldea, and L. E. Unnewehr, Permanent Magnet, Reluctance and Self-Synchronous Motors. Boca Raton, FL: CRC, 1993.

[12] G. C. D. Sousa, B. K. Bose, J. G. Cleland, "Fuzzy Logic Based On-Line Efficiency Optimization of an Indirect Vector-Controlled Induction Motor Drive", *IEEE Trans .on Ind. Elec.*, Vol.42, No.2,pp. 715-722, July/Aug. 1986.

[13] J. Lau and M. N. Uddin, "Non linear adaptive backstepping based control for IPMSM drive," *International Electric Machines and Drives Conference, San Antonio TX, USA*, pp. 1689-1694, 2005.

[14] B. Sneyers, D. W. Novotny, and T. A. Lipo, "Field weakening in buried magnet ac motor drives," *IEEE Trans. Ind. Appl.,* Vol.IA-21,pp. 398-407, Mar./Apr.1985.

[15] Zhou, Keliang and Wang, Danwei " Relationship between Space-Vector Modulation and 3-phase carrier based PWM: A comprehensive analysis", *IEEE Trans. Industrial Electronics*, Vol. 49, No. 1, pp.478-485,Feb. 2002.

[16] R. J. Kerkman, T. M. Rowan, D. Leggate, and B. J. Seibel, "Control of PWM voltage inverters in the pulse dropping region," in *IEEE-APECConf. Rec.*, pp. 521–528, 1994.

[17] H. W. Van Der Broeck, "Analysis of the harmonics in voltage fed inverter drives caused by PWM schemes with discontinuous switching operation," in *European Power Electronics Conf. Rec.*, pp.261–266, 1991.

[18] J. Holtz, "Pulsewidth modulation for electronic power conversion,"*Proc. IEEE*, pp. 1194–1214, Aug. 1994.

[19] S. Ogasawara, H. Akagi, and A. Nabae, "A novel PWM scheme of voltage source inverter based on space vector theory," in *European Power Electronics Conf. Rec.*, pp. 1197–1202, 1989.

[20] F. Abrahamsen, J. K. Pedersen, F. Blaabjerg: "State-of-Art of Optimal Efficiency Control of Low Cost Induction Motor Drives", *Proceedings of PESC'96*, pp. 920-924, 1996.

[21] Fidel Fernhndez-Bernal, Aurelio Garcia-Cerrada, Roberto Faure, "Loss-minimization control of synchronous machines with constant excitation," *IEEE Power Electronics Specialists Conf* (PESC'98), Vol. 1, pp.132- 138, May.1998.

[22] Slobodan N. Vukosavi} "Controlled Electrical Drives - Status of Technology", *Zbornik XLII Konf. ETRAN-a*,rnja~ka Banja, 2-5 juna 1998, Sveska 1, str. 3-16.

[23] A.Fratta, A.Vagati, EVillata, "Design Criteria of an IPM Machine Suitable for Field-Weaken Operation", *Proceedings of the International Conference on Electrical Machines*, pp. 1059-1065,1990.

[24] Shigeo Morimoto, Yi Tong, Yoji Takeda, Takao Hirasa, "Loss drives minimization control of permanent magnet synchronous motor," *IEEE Trans. Industrial Electronics,* Vol. 41, No. 5, pp. 866– 871, Sept./Oct.1990.

[25] B. K. Bose, "A high-performance inverter-fed drive system of an interior permanent magnet synchronous machine," IEEE *Trans. Ind. Appl.,* vol.IA-24, pp. 987-997, Nov./Dec. 1988.

[26] T. M. Jahns, "Flux-weakening regime operation of an interior permanent-magnet synchronous motordrives," *IEEE Trans. Ind. Appl.,* vol. IA-23, pp. 681489, July/Aug. 1987.

[27] Patrick L. Jansen, and Robert D.Lorenz, "A Physically Insightful Approach to the Design and Accuracy Assessment of Flux Observers for Field Oriented Induction Machine Drives", *IEEE Trans.Ind.Applicat*,vol.30, No.1, Jan, 1994.

[28] Y.HondaY H.Murakami, K.Narazaki, T.Higaki,S.Morimoto, Y.Takeda, "Optimum Design of a Multi Layer Interior Permanent Magnet Synchronous Motor Using

Reluctance Torque", *Electrical Engineering in Japan,* vol.127, No.1, pp.249-259, April **15,** 1999.

[29] W.L.Soong, T.J.E.Miller, "Design of a New Axially Laminated Interior Permanent Magnet Motor", *Proceeding of annual meeting of IEEE Industrial Applications Society,* pp.27-36, 1993

[30] W.L.Soong, T.J.E.Miller, 'Theorical Limitation to the Field Weakening Performance of the Five Classes of Brushless Synchronous AC Motor Drive", *Proceeding of the Electrical Machines and Drives Conference in Oxford,* pp.127-132, September 1993.

[31] T.A.Lipo, A.Vagati, L.Malesani, T.Fukao, "Synchronous Reluctance Motors and Drives - A New Alternative", *IEEE/IAS 27th Annual Meeting, Tutorial Course, Electric Machine Committee,* 1992.

[32] Matlab, *Simulink User Guide.* The Mathworks Inc., 2004.

[33] dSPACE, *Implementation Guide.* Germany: Paderborn, 2003.

[34] V. R. Stefanovic, "Static and dynamic characteristics of induction motors operating under constant air-gap flux control," IEEE IAS Annu. Meeting,pp.511-517, Oct. 1976.

[35] Marko Hinkkanen and Jorma Luomi, "Parameter Sensitivity of Full-Order Flux Observers for Induction Motors", *IEEE Trans.Ind.Applicat,* vol.39, No.4, Jul/Aug, 2003.